MULTI-OBJECTIVE AERO/MECHANICAL DESIGN OPTIMIZATION
OF GP TURBINE BLADES PLATFORM CONTOUR USING ADJOINT
SOLVER AND IMPACT ON SECONDARY LOSSES

by

MOSTAFA SOLIMAN

DISSERTATION

Submitted to the Faculty of the Graduate School of The University of
Texas at Arlington in Partial Fulfillment of the Requirements for the Degree of

DOCTOR OF PHILOSOPHY

THE UNIVERSITY OF TEXAS AT ARLINGTON

August 2022

ACKNOWLEDGEMENTS

LIST OF FIGURES

LIST OF TABLES

LIST OF ABBREVIATIONS AND NOMENCLATURE

CFD   Computation Fluid Dynamics

GP   Gas Path

HGP   Hot Gas Path

HCF   High Cycle Fatigue

HTC   Heat Transfer Coefficient

HP   High Pressure

IC   Internal Combustion

ICE   Internal Combustion Engine

IP   Intermediate Pressure

LCF   Low Cycle Fatigue

LP   Low Pressure

MFR   Mass Flow Ratio

PS   Pressure Side

PSP   Pressure Sensitive Paint

SS   Suction Side

TBC   Thermal Barrier Coating

TSP   Temperature Sensitive Paint

TE   Trailing Edge

LE   Leading Edge

T_t Total Temperature

P_t Total Pressure

M   Mach Number

γ Cp/Cv

Cp   Specific Heat Coefficient at Constant Pressure

Cv   Specific Heat Coefficient at Constant Volume

ΔP   Delta Pressure

EDM   Electrical Discharge Machining

DR   Density Ratio

N   Number of Blades

B.Cs   Boundary Conditions

MCS   Modal Cyclic Symmetry

HGP   Hot Gas Path

ABSTRACT

Multi-Objective Aero/Mechanical Design Optimization of GP Turbine Blades Platform Contour

Using Adjoint Solver and Impact on Secondary Losses Method

Mostafa M. Soliman, Ph.D.

The University of Texas at Arlington, 2022

Supervising Professor: Dereje Agonafer

Gas turbines HGP (Hot Gas Path) components represent the major contribution to generating power in gas turbines as they are the components that mainly extract power from hot gases that come out of the combustion chamber (Combustor). Due to harsh environment and high temperature, these components are vulnerable to high thermal and mechanical stresses which affect its durability, life, and efficiency. Hot gases go through these components can reach very high max temperature. Max blade alloy metal temperature in GP (Gas Path) blades can reach 1800-1900 F. Because of these severe operation conditions, a very careful prediction of stresses, thermal distribution, losses, and flow characteristics need to be studied in depth to focus more into variables and factors that can affect gas turbine's hot gas path components durability, living & efficiency.

In many research studies, it has been noted the impact of purge flow and platform contour near the endwall for nozzle and platform blades on the overall secondary losses and specifically on the horseshoe vortex that can be formed near the hub of the blade and nozzles, which can increase turbulence and cause lower thermal efficiency. It was also found that one of the main

reasons of horseshoe vortex formation and intensity is the ΔP value between PS and SS near the blade aerofoil hub that can control the lateral flow component that migrates from PS to SS and this cause an increase of vortex intensity which will contribute on platform temperature increase which will consequently lower the GP (Gas Path) component life and crack initiations capability that could propagate and even increase the losses further more.

The focus of this study is GP turbine blades platform contouring impact on secondary flow and losses near platform surface using adjoint solver optimization tool in order to lower the pressure difference between PS (Pressure Side) and SS (Suction Side) near the hub as much as possible to control vortex and turbulence near the platform surface caused by lateral flow component. Used for the study, GP second stage blade internally cooled with a serpentine core where flow exits from blade tip and through TE ejections. GP (Gas Path) components are apparently critical components in design and analysis to capture as accurate as possible factors, variables, and unknowns that might impact the component's performance and durability. Currently, it has been reported by many gas turbine's manufacturers during engine inspection signs of failures and shortfall of durability in GP blades, in addition to the failures that can cause engine shutdown. After investigating and going through inspection reports on many GP (Gas Path) blades that came from the field for damage inspection, some consistent cracks and damage have been noted in the platform section at multiple locations of the blades, and that is the area of focus during this study. After further investigation we came to a conclusion that one of the major reasons has been known for platform crack initiation is the thermal gradient through the blade, especially in the platform-aerofoil root area which can imply tremendously high thermal stresses at some specific locations that can eventually cause a crack initiation at these critical locations.

The first part of this study will be focusing on building Computation Fluid Dynamics (CFD) model with adaptive mesh method that will allow to get the most accurate results as possible for the baseline blade platform with a flat surface same scale of the linear cascade that will be used on the blade test for a blade flow passage. The boundary conditions that are most represent the real model, are applied in addition the linear periodic boundary conditions that represents a one blade passage and flow conditions such as pressure, temperature, inlet mass flow rate for mainstream, inlet mass flow for purge flow and flow exit conditions. The result of this study will be a baseline pressure distribution for a blade flat platform near the hub and a very accurate focus on the pressure at the hub location of intersections edges of blade platform with aerofoil PS and SS edges. ΔP value will be then calculated to represent the average static pressure value for the PS platform edge subtracted by the average static pressure value of the SS platform edge, this will represent the ΔP for the baseline flat platform blade.

The second part of the study was focusing on optimization for the baseline blade platform non-axisymmetric contour that will lower the overall ΔP value between the PS and SS edges to lower the lateral flow component for three different contours and adjust the mesh after each iteration for data validation. The outcome of this study showed that non-axisymmetric contour on blade platform can have a tremendous impact on static pressure at PS and SS edges near the hub that we have three different geometries with pressure reduction of 5%, 10%, and 20%. The mesh has been adjusted and the model has been validated with an updated CFD model run with modified contour mesh and it was in agreement with the optimizer's initial estimate.

TABLE OF CONTENTS

CHAPTER 1

INTRODUCTION

Gas turbines for the purpose of generating electricity were used for the first time in the late 1930s. Gas Turbines then became widely used in energy production technologies in our age [1]. Gas Turbines can operate with many different fuel sources such as diesel fuel, methane, natural gas, crude and biomass gases. Technologies for these turbines have improved in many aspects since the 2000s, notably material and alloys capabilities, equipment design techniques, systems controls and new coatings which allowed axial compressors in gas turbines to run with much higher compression ratio, increasing from 7:1 to 45:1 compression ratio, which lead to a direct increase in single-cycle gas turbine efficiency from 15 percent to 45 percent in some gas turbines [2]. Table 1 shows thermal efficiency and economical comparison for different engines that are running with different type of fuel from the initial cost to the operating cost of these gas turbines, from provided data it is revealed that the economics of power generation depend on the fuel cost, maintenance and engine overhauling and operating efficiency [3].

Table 1 Economic Comparison of Various Power Generating Technologies

Technology Comparison	Diesel Engine	Gas Engine	Simple Cycle Gas Turbine	Micro Turbine	Fuel Cell	Solar Energy Photovoltic Cell	Wind	Biomass	River Hydro
Product rollout	Available	Available	Available	Available	Available	Available	Available	Available	Available
Size range (kW)	20–100,000+	50–7,000+	500–450,000+	30–200	50–1,000+	1+	Up to 5,000	Up to 5,000	20–3,000+
Efficiency (%)	36–43%	28–42%	21–45%	25–30%	35–54%	NA	45–55%	25–35%	60–70%
Gen. set cost ($/kW)	125–400	250–600	300–600	800–1,200	1,500–3,000	NA	—	NA	NA
Turnkey cost No-heat recovery ($/kW)	200–500	600–1,000	400–850	1,200–2,400	2,500–5,000	5,000–10,000	700–1,300	800–1,500	750–1,200
Heat recovery added cost ($/kW)	75–100	75–100	150–300	100–250	1,900–3,500	NA	NA	150–300	NA
O&M cost ($/kW h)	0.007–0.015	0.005–0.012	0.003–0.008	0.006–0.010	0.005–0.010	0.001–0.004	0.007–0.012	0.006–0.011	0.005–0.010

*The above information is based on data obtained from several sources such as manufacturers and technical magazines.

Gas turbines are a type of internal combustion engine (ICE) in which compressed air ejects from an axial compressor and is then mixed with fuel to form high-pressure air-fuel mixture, which when ignited it is producing hot gases that pass through the multi-stage power turbine to generate and extract energy from the exhaust hot gases, and convert them into rotational power to the turbine's rotor. Gas turbines can use a wide range of fuel types such as natural gases, fuel oil and synthetic fuels and many similar fuels. While combustion takes place intermittently in reciprocating internal combustion (IC) engines, a continuous combustion takes place in gas turbines.

Compressed air is getting mixed with fuel injected through a fuel nozzle before being pushed into the combustor where it is ignited and generates hot gases at constant pressure, after which the high-pressure hot gases pass through the power turbine. The power turbine consists of numerous rows of fixed nozzle stages that direct the hot pressurized gases to multi blade rotor stages in order to extract as much momentum energy as possible from the high-pressure hot exhaust gases that impart rotational and rotational power to the turbine's rotor. The shaft's rotation is responsible for powering the multistage axial compressor, which continuously draws air into the compressor to keep and maintain continuous combustion and energy generation. The shaft of the turbine is also coupled with the generator by clutches or gear box to use the rest of the rotational energy to produce electrical power. About half of the produced Gas Turbine power is used to power the compressor, and the rest is used for energy generation. More than one compressor and power turbine stages can be used to generate more power and increase the efficiency of the Gas Turbine in terms of kinetic energy extraction optimization for hot gases.

Figure 1 GE Heavy Duty 9HA Frame Unit

1.1 Categories of Gas Turbines

Simple Cycle Gas Turbines are basically grouped into four classes. These are:

- Frame Heavy Duty Gas Turbines

- Aero-Derivative Gas Turbines

- Industrial Gas Turbines

- Small Gas Turbine

1.1.1 Frame Heavy Duty Gas Turbines

Frame Heavy Duty Gas Turbines are large-scale gas turbines with efficiencies ranging from 30 to 48 percent and capable of producing power from 3 to 480 MW in a single cycle configuration.

1.1.2 Aero-Derivative Gas Turbines

Aero-Derivative Gas Turbines use aviation-derived engines such as GE LM 6000, LM 2500, TM 2500 and LMS 100 as the main power generation source these turbines can run with efficiencies ranging from 35 to 45 percent and producing power between 2.5 and 100 MW.

1.1.3 Industrial Gas Turbines

Industrial Gas Turbines, which are generally used as a mechanical drive train in petrochemical and oil production facilities, this type of gas turbines run with an efficiency ranges 30s percent and capable of producing power between 2.5 and 15 MW.

1.1.4 Small Gas Turbine

Small Gas Turbines, which generally have a centrifugal compressor and a radial inlet turbine, are gas turbines with an efficiency of 15 to 25 percent in a single cycle configuration and capable of producing power between 0.5 and 2.5 MW.

1.2 Main Components of Gas Turbines

In this section, an overview for the main components of the Gas Turbines and Jet Engines that will be presented as following.

1.2.1 Hot Gas Path Components Overview

Hot Gas Path components are the components that interacts with the hot gases, these components have a high importance because it is exposed to harsh environments conditions which requires it to be carefully designed against these conditions. The main concern in the Hot Gas Path is the high temperature and high-pressure gasses operating conditions, the gas temperature leaves the combustor and approaching the nozzle with very elevated firing temperature that can raise the nozzles and blades metal temperature to above 1800 F, in addition to the hot gases pressure that's applied to the nozzle and blades surfaces , thus conditions can have an enormous thermal and mechanical stresses on Gas Path Components which may lead to a crack initiation, material creep & vibrations which can cause a severe irreversible damage to the stationary components (Nozzles, Shrouds), rotational components (Blades, Rotor) that will cost a lot of money and cause long gas turbine downtime.

1.2.2 Combustion Chamber (Combustor)

Figure 2 Optimal Failure-Finding Intervals for Heat Shields in a Gas Turbine Combustion Chamber Using a Multicriteria Approach [4]
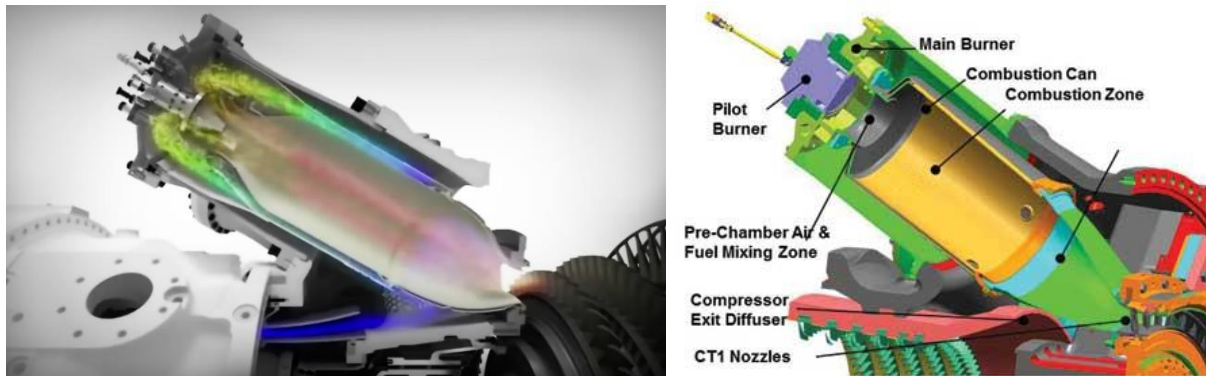
Note: DLE combustion arrangements tend to be can-annular or annular combustion configuration.

Figure 3 DLE Combustion System Design 2000 [5-6]

Combustor or the combustion chamber is the stage where the pressurized air that exits from compressor is mixed with the fuel and gets ignited to generate the hot exhaust gases with high momentum energy.

1.2.3 Nozzles

The stator guide vanes or called nozzles are convex and concave and have an aerofoil shape, the main purpose of these guide vanes is to direct the combustion gases coming out of the combustion chamber (Combustor) to the turbine blades and also converting the high pressure gas energy that is contained in the exhaust gasses to kinetic energy by accelerating the flow going to

the blades rotating stage, while gasses passes through the nozzles are given a swirl in the direction of the rotation of the turbine rotor blades, causing the turbine to rotate at a high speed. Nozzles must be highly engineered and designed because they are the first components to contact hot gases immediately after combustion, Therefore, it is considered the hottest gas path components and are vulnerable to failure due to harsh thermal conditions.

Figure 4 First Stage Air-Cooled Turbine Nozzle Segment [7]
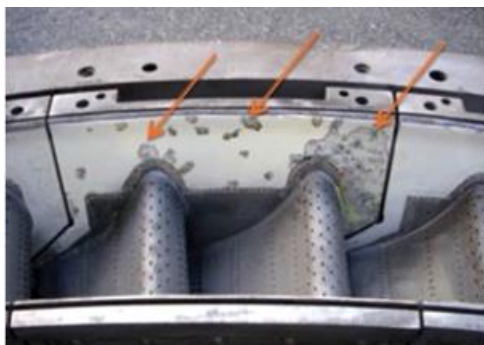
a) Contaminated TBC was found on a first-stage nozzle during final inspection

b) First-stage nozzles took a beating on this 7FA in cogeneration service.

Figure 5 Contaminated TBC on First-Stage Nozzle [8]

Figure 6 Stage One Nozzle [9]

1.2.4 Blades

It is the stage that rotates in the gas turbine and extract energy from the flow and converts it into mechanical rotation that can generate power. The blade is shaped as a concave-convex aerofoil shape, that is fixed on a plate called blade platform. The blades are attached to a rotating disk with firtree shaped couplings to ensure they are secured during rotation and can withstand the applied mechanical stresses.

Since the blades are the parts that rotate at speeds that can range between 3000-13000 RPM in the gas turbine, and even at higher speeds in other jet engines, they are the parts that are exposed to the highest thermal and mechanical stresses combined. Besides mechanical stress, blades are also exposed to high temperature exhaust gases, which lead to an increase in the blade's metal temperature that can go above 1800 F. Because of these extreme challenging mechanical and thermal conditions, factors that is likely to affect blade's temperature must be carefully optimized for a better overall blade life and durability. This study will focus on the platform surface contour of the GP blades and its effect on the pressure distribution near the second stage GP blade platform surface.

Blades are most affected by damage mechanisms that comes from LCF (low cycle fatigue), creep, HCF (high cycle fatigue), oxidation and hot corrosion. These are described in the following sections.

1.2.4.1 Low Cycle Fatigue

It is so named because fatigue failure occurs at lower cycle count. It is the most common type of fatigue failure that can occur from engine start-shutdown cycle. Each time the engine getting started, a certain amount of thermal and mechanical stress is applied. This stress is gets reversed during the hot to cold condition when the engine is turned off, repeating that behavior repeatedly can expose the material to a high fatigue stress that can cause a crack initiation that can result in blade failure and engine breakdown.

1.2.4.2 High Cycle Fatigue

It is so named because fatigue failure occurs at a high number of cycles. This is associated with vibration and resonance damage caused by the intersection of mode drivers and failure modes at the full load operation.

1.2.4.3 Creep

This type of failure is caused by a constant thermal and mechanical stress that is applied to the blade for a long period of time, since the blade are getting hot and the mechanical stress will always be applied due to rotation and hot gasses pressures over the surface of blades and nozzles, that can cause the blade alloy to creep and can lead eventually to a creep rupture that can cause an engine failure

1.2.4.4 Oxidation and Hot Corrosion

This type of failure has been seen in harsh environments where engines are operating at salty or sulfuric environment that can cause damage to the blade TBC (Thermal Barrier Coating)

and eventually damage the blade nickel alloy, this damage will be accelerated with higher

temperatures. Some pictures for GP turbine blades and possible blade failures due to fatigue,

creep and corrosion during operation are given below as examples.

Figure 7 GE Frame 5 Stage 1 Blade [10]
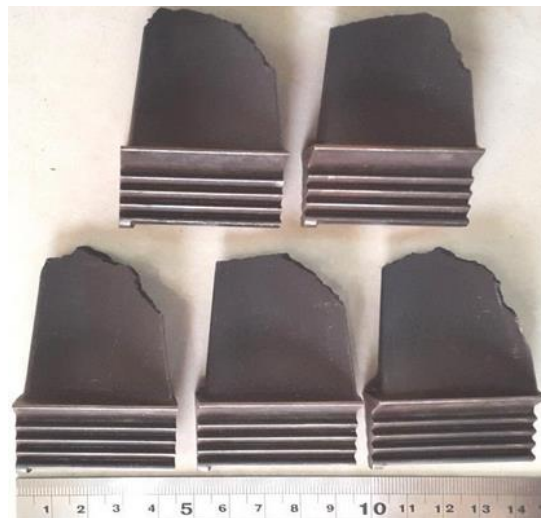
Figure 8 Damaged Rotor Blades of First-Stage Turbine Blades After 6500 Hours of Operation at
About 750-800 deg C a 6.5 MW Gas Turbine [11]
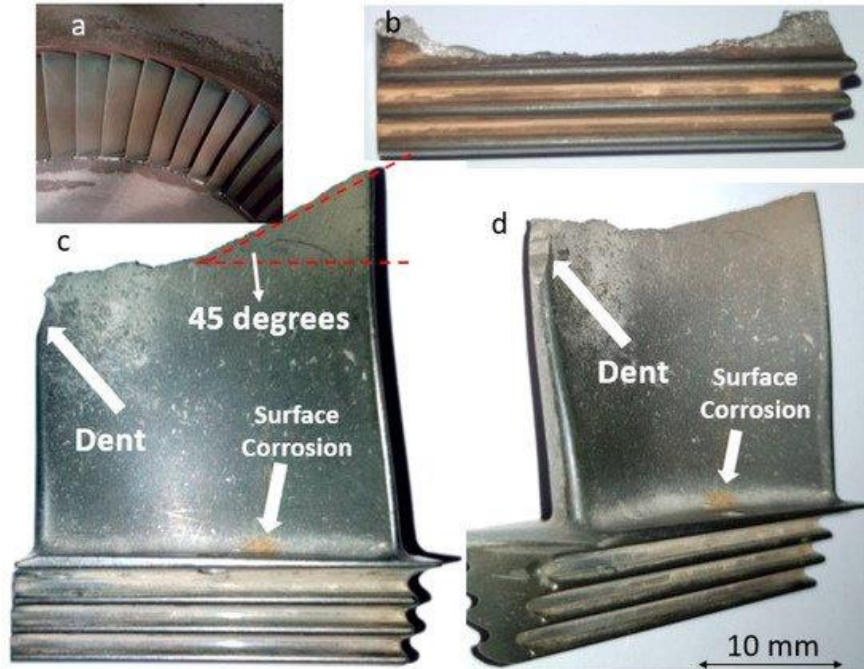
Figure 9 Visual Observation of Broken Blade, (a) Overview of Blades in The Assembled Condition, (b) Failed Blade From The Root, and (c,d) Broken Blade From The Airfoil [12]
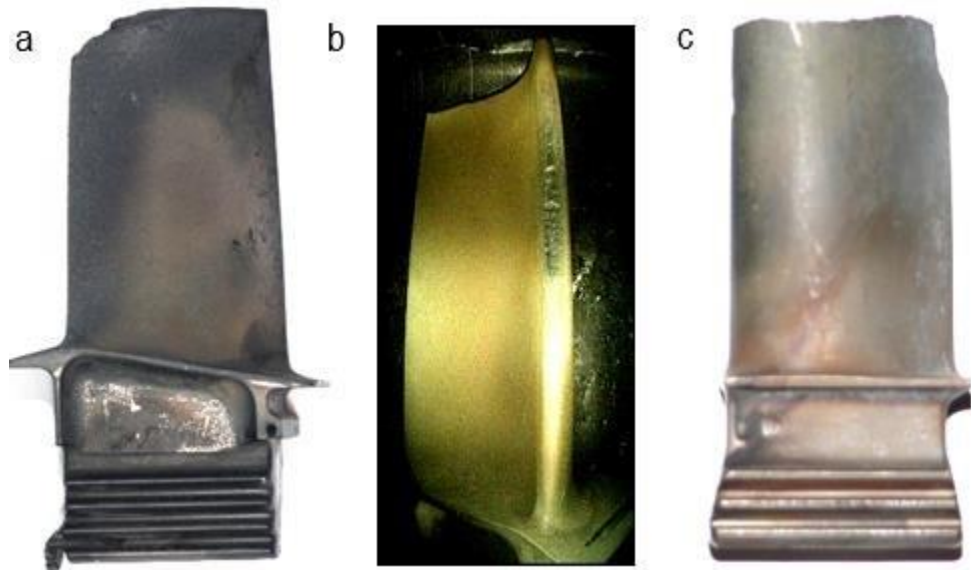
Figure 10 Instances of Thermal Damages to Gas Turbine Blades: a) The Region of Material Overheating at The End of The Leading Edge, b) Overheating Region and a Fracture on The Leading Edge, c) The Blade Broken Off Due to Material Overheating [13]

In modern gas turbines, the turbine inlet temperature is constantly pushed upwards to achieve a higher power generation and turbine efficiency. Higher temperatures and flatter temperature profiles have made blade's platform cooling a necessity of overall turbine cooling design. Platform cooling uses a combination of stator rotor bleed or purge discharge flow and discrete orifice film cooling holes that is machined on the surface of the platform to form a film cooling on the blade's platform. The cooling process on the platform is quite difficult due to the presence of three-dimensional flow structures at the blade passage [14].

1.3   Blade Cooling and Effect in Efficiency & Durability

As explained earlier Hot Gas Path components are running under critical conditions firing exhaust temperature from 2000- 2600 F firing temperature, which can expose the blade alloy to an extreme temperature as explained earlier, that means without proper cooling to the GP blades we cannot push the engine beyond limits with a higher power generation and efficiency, and eventually blades will fail due to creep, fatigue and hot corrosion from applied thermal and mechanical stresses. The target always for GP components is to achieve a lower metal temperature with a lower gradient at full load steady state condition and during start-shutdown transient cycle. During the design process the percentage of air to be injected for cooling is budged out of overall engine's performance, tradeoff studies are being carefully considered to determine the percentage of cooling air needed with the firing temp in order to achieve efficiency and power targets.

GP Turbine blades platform profile affects performance loss and can cause an engine failure, near wall platform secondary losses generated by circumferential flow from PS to SS due to pressure difference can lead to turbulence increase near the platform that increase the HTC value and cause a rise in temperature which can be damaging to the blade platform surface and

11

eventually cause cracks to start. Focusing on the platform surface of the blades, there is a purge

flow, also called bleed discharge flow, which is injected through the gap between the nozzle

stator and the blade rotor stages and acts as a layer on the upper surface of the platform that

separates hot exhaust gases from the platform surface, that lowers overall platform temperature

and increase blade's durability as shown in Figure 12.
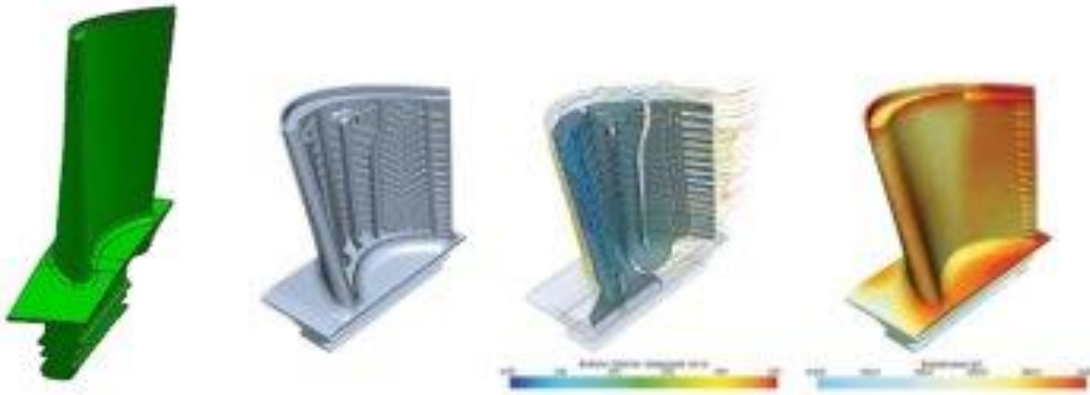
Figure 11 a) GP Second Stage Turbine Blade, CFD Simulation of Gas Turbine Blade Cooling
Showing b) Blade Cutaway View c) Cooling Air Pathway and Streamlines d) Blade Surface
Temperature [15]

Blade's mechanical reliability is greatly affected by the thermal distribution on the blade

platform that must be very carefully addressed because it is in a direct correlation with creep

capability hours with higher platform surface temperature, and also related to fatigue capability

due to higher temperature gradient over platform surface.
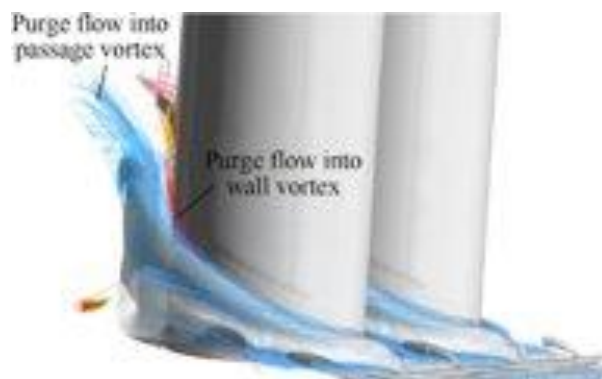
Figure 12 Purge Flow Injection Over Platform Surface [16]

Regarding secondary loss near platform, the flow field near the hub endwall region of the blade passage is dominated by the boundary layer, strong pressure gradients, and cross flow in the pitch wise direction from the pressure side to the suction side. When the endwall boundary layer approaches the blade row, a vortex is formed near the junction of the blade leading edge and the endwall. This vortex is termed as the leading-edge horse-shoe vortex. The horse-shoe vortex splits at the leading edge and propagates downstream into the passage on both the pressure side and the suction side of the blade passage forming two legs of the early passage vortex flows.
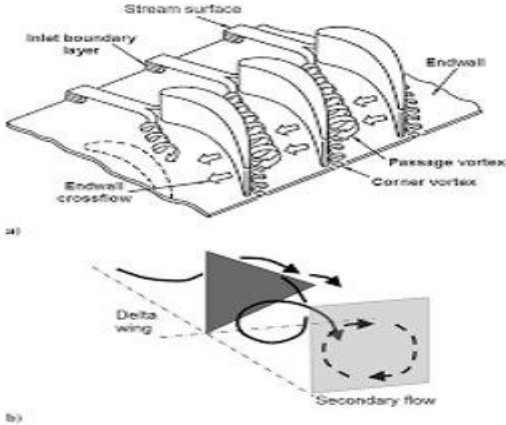
Figure 13 Near Platform Vortex [17]
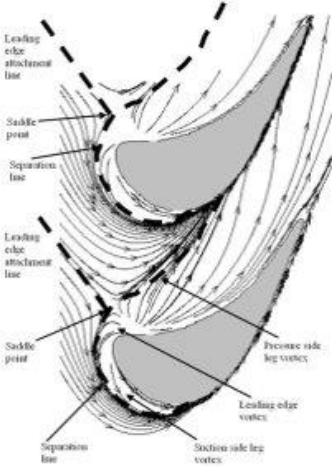
Figure 14 Streamlines Showing Separation Lines in a Near Endwall Plane of a Linear Blade Passage [18]

It has been clearly demonstrated in Figure 14 that one of the main factors affecting the horse-shoe's vortex formation and vortex intensity is the lateral flow component from the PS near the hub to the SS near the hub. This study will focus on limiting this lateral/circumferential flow component in order to limit the intensity and size of the horseshoe vortex near the platform surface that leads to lower platform temperature and higher engine's efficiency.
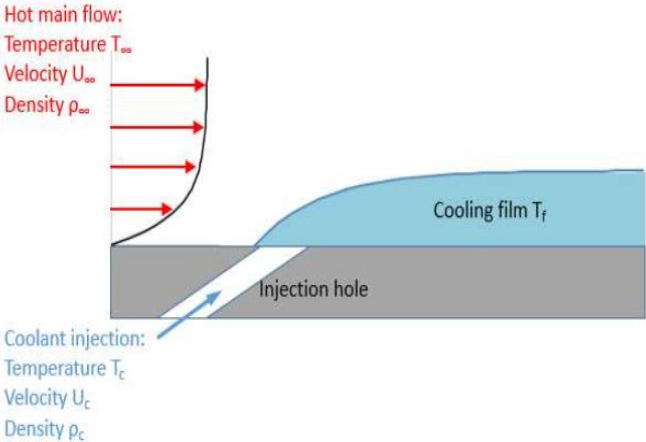
Figure 15 Platform Purge Flow Film Cooling and Main-Stream Flow [19]
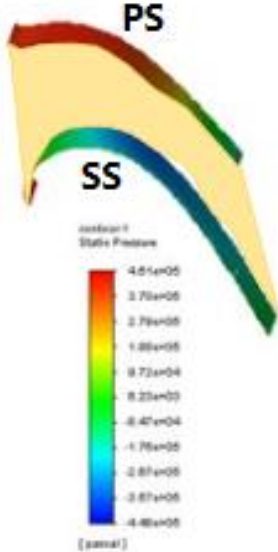
Figure 16 Near Platform PS and SS Pressure Distribution

As shown in the Figure 16, for the engine to generate power the PS average pressure need to be always higher than the average pressure for the SS to create a pressure difference that can rotate the engine's rotor shaft and generates energy, that is one of the main reason behind why this lateral flow component is formed as the flow go axially the intensity of the vortex is increasing as explained with details in previous literatures review in the next chapter.

CHAPTER 2

LITERATURE REVIEW

We went in depth in this section on the literature review for impact of platform contouring or endwall contouring for nozzles on film cooling effectiveness either on nozzle endwall surface or blade platform surface, in addition included literature review on flow structure near endwall for both nozzles and blades.

Since the 1970s, there has been a steady increase in the thermal efficiency of gas turbine engines as a result of the increase in turbine inlet temperature. For higher thermal efficiencies, gas turbines are operated at first stage inlet temperatures of around 1500°C. This results in extreme thermal stresses on gas turbine HGP components as previously explained. When operating continuously with high turbine inlet temperatures, further thermal failure of hot gas path components may occur. In addition, since the gas exiting the combustion chambers is not always distributed uniformly, it will increase the temperature exposure on the rotor platform. This situation requires effective thermal protection measures.

Film cooling is described as an external cooling technique that is often used in conjunction with internal cooling to protect turbine components from mainstream hot gases exhaust, some of the coolant used for internal cooling is expelled through slots or separate EDM manufactured holes on the surface of components that need thermal protection to act as a barrier layer between the metal and hot gasses. The coolant discharged in this way replaces the mainstream boundary layer, forming a protective film on the surface of the exposed component. This isolates the hot main gas from the metal surface, significantly reducing the temperature level of the metal alloy surfaces and overall hot gas path components.

There has been lots of work and studies focused on nozzles endwall and some were also presented studies done to blade platform surfaces that has a great impact on cooling effectiveness and overall aerodynamics losses and secondary flow losses near the hub.

2.1 Nozzle Endwall and Blade Platform Film Cooling Effectiveness

Langston and his colleagues [3, 19-20], Chyu [21], and Simon and Piggush [22] have showed flow structures and their impacts on film cooling and heat transfer in some of their studies. The studies of these researchers show that the small-scale horseshoe vortex turned into a much larger transitional vortex as it migrated from the leading edge of the blade to the suction side of the adjacent blade. It has been noted also that several small-scale corner vortices also occur near the intersection of the turbine blade surface and the platform surface.

The platform surface is mostly cooled by draining the coolant through separate holes. The film cooling process in endwalls with separate cylindrical holes has been investigated by many researchers. In Takeishi et al.'s [23] study, heat transfer and film efficiency distributions were obtained in a vane endwall with film holes placed at three different locations in the passage. In Harasgama and Burton's [24] study, film cooling was used near the leading edge, just inside the transition where the film cooling holes are located. The film cooling configuration that Jabbari et al. [25] used, appears to consist of discrete holes located in the downstream half of the passage.

The efficiency of film cooling and aerodynamic loss in a fully film cooled endwall were studied in detail by Friedrichs, Hodson and Dawes [26-28]. The aforementioned literature studies have shown that the film cooling efficiency is strongly affected surface of the end wall secondary flows and turbulence. The cooling flow is carried from the pressure side to the suction side of the passage by the cross flow. It was also noted that when film holes are placed on the separation line of the secondary flow, the coolant tended to lift off. Because the horseshoe vortex is rolled,

the front of the endwall portion is not easy to cool with film holes. Coolant can also be supplied from the gap between the nozzle vane stator stage and the blade rotor stage. This ensures that the cooler prevents hot mainstream gas from entering the disk cavity and can provide some more cooling to the front platform area throughout the process. Research by Blair [29] about half a century ago showed that secondary flows significantly alter the film cooling efficiency for upstream slot ejection throughout the transition. Slot cooling in the endwalls surfaces have been demonstrated by many researchers [30-36]. It has been shown in these studies that the upstream slot cooler not only was capable of cooling turbine blade leading edge, but also reduces the strength of the secondary flows in the passage by increasing the momentum of the boundary layer of the incoming main flow. Delta wings were used by Wright et al. [37] in a low velocity linear cascade and by Gao et al. [38] in a high velocity cascade to examine the effect of upstream vane endwall passage vortex on discharge flow cooling. In these studies, it has been shown that the vortex created by the delta wing has a very negative effect on the discharge flow cooling.

Research conducted by Suryanarayanan et al. [39] to investigate platform slotted discharge flow cooling in a three-stage turbine rotation facility, found that the interaction between the stator and rotor stator also affects the platform film cooling efficiency. In actual practice, cooling of the platform is done by either the upstream slot or the separate hole film cooling. In Nicklas' study [40] it was found that he used three rows of film cooling holes in the front third of the endwall as well as a slot. It was found that the passage vortex sweeps the cooling flow which made it very difficult to cool the downstream passage and the pressure side corner with such an arrangement. In the study by Wright et al. [41], in which the layout design of the film holes was made in the blade platform's throat region, the entire platform was cooled efficiently but with using a high amount of coolant flow.

The combined cooling technique consisting of two and four rows of cylindrical and "shaped holes" was used by Gao, Narzary and Han [42] to investigate four different discrete hole patterns. In the related study, it was found that the best film cooling and aerodynamic performance was achieved with shaped holes, while the two- and four-row layouts did not show any significant difference in the lateral average efficiency. In a study by Suryanarayanan et al. [39] examining combined film cooling in the same rotating facility as used in one of their previous studies [43], it was found that increased discharge flow rate and rotation speed increased film cooling efficiency. In the related study, it was found that for the downstream discrete apertured film cooling, a native blowing ratio of 1.0 offered the best level of film coverage and efficiency [43].

Most studies on film cooling have used cooling flow to mainstream density ratio (DR) of around 1.0. However, this ratio is far from the true density ratio of about 2.0 that occurs in real turbines due to the temperature difference between the cooling flow and the hot main-stream.

There were many early studies of flat plates with simple angled holes. Strong dependence of film cooling effectiveness was shown by Wright, Black and Han [44] when the density ratio varies in the range of 0.75-4.17 on a flat plate with holes inclined at 35 degrees. A cooling hole of similar geometry and a density ratio ranging from 1.2 to 2.0 were used by Pedersen, Eckert, and Goldstein [45]. In the related study, it was found that at low blowing mass flow rates, the efficiency scales well with the mass flux ratio, and with higher blowing mass flow rates, the efficiency scales well with the momentum flux ratio. In both studies mentioned above, it was found that the maximum adiabatic efficiency increased with increasing density ratio. Experiments were performed on the vane suction side using low and high density cooling flow ratios by Sinha, Bogard and Crawford [46]. Findings from these experiments showed that holes

on the suction side of a strong curvature have a much higher efficiency than holes with a similar injection angle on a flat plate. Research by Ethridge, Cutbirth, and Bogard [47] found that optimum blowing rates over a blade surface were 0.8 when using air as the coolant and 1.2 when using CO2 for cooling. The level of turbulence in the incoming main-stream also affects platform cooling, and combustion chamber design can change this effect.

It is seen that there are many studies on flat plates in the literature on this subject. In studies by Ekkad et al [48], Kadotani and Goldstein [49], and Jumper, Elrod and Rivir [50], it was found that the film cooling effectiveness decreased at high turbulence levels at low and medium blowing ratios but increased at high blowing rates due to the cooling liquid dispersion.

In all of these studies, it is seen that the turbulence intensity varies between 0.3% and 20.6%, and the cooling flow to mainstream flow density ratio is around 1.0. Bons, MacArthur and Rivir [51] also obtained similar findings using a high coolant-to-mainstream density ratio of 2.0. It was also confirmed by Schmidt and Bogard [52] that the geometry of the cooling hole changes the effect of turbulence density on film cooling effectiveness. In their study, they found that holes with smaller L/D ratios were more subject to turbulence levels than those with larger L/D ratios [52]. Another study [53] found that, unlike cylindrical holes, shaped holes did not show improved efficiency at high turbulence levels. Narzary et al. [14] used a high-pressure turbine rotor blade platform to investigate the film cooling effectiveness by independently changing four critical parameters (parameters such as 1-Free flow turbulence level, 2-Discharge flow rate, 3-Blowing rate, and 4-Cooling flow to-mainstream density ratio, each within typical ranges for the actual engine operating condition). In previous studies on this cascade, it is seen that Pressure Sensitive Paint (PSP) technique is used for film cooling with a density ratio close to 1.0 and a low free flow turbulence density of 4.2%. However, it should be noted that the PSP

technique is limited to film cooling efficiency measurements only. The technique of Temperature

Sensitive Paint (TSP), on the other hand, is a broader application technique that can be applied to

both film cooling and heat transfer measurements. This study performed was a two-stage study

involving film cooling and heat transfer coefficient, the TSP technique was used instead of PSP

technique. When the results obtained were compared with those obtained from the PSP test

performed under the same experimental conditions, the findings were found to be reasonably

consistent [14].

2.2 Impact of Vane Endwall and Blade Platform Surface Geometry and Contour on Film Cooling Effectiveness

Praisner and Smith [54] discussed the dynamics of the horseshoe vortex as well as the

effect on endwall heat transfer around the Leading Edge near the endwall. Zhang and Yuan [55],

Zhang, Yuan and Ligrani [56], Mahmood, Gustafson and Acharya [57], Han and Goldstein [58]

focused their study on the effect of Vane Leading edge fillet size and shape and infiltration blow

rate on horseshoe vortex, which would affect secondary flow and film cooling efficiency. Here,

the cooling efficiency they offer this form of Leading edge and Leading-edge fillet also has a

major impact on secondary flow losses and film cooling near the end wall. In the study of Zhang

and Jaiswal [35], the effect of the film cooling efficiency on the end-of-wall infiltration flow was

tried to be determined experimentally by using the PSP method. Findings from these studies

showed that secondary flows near the end wall strongly affect GP blades, Platform surface and

Nozzle end wall surface heat transfer and film cooling. This, in turn, will have a major impact on

the heat transfer coefficient near the end wall, which will subsequently affect the film cooling

efficiency. From this it should be understood that deliberately designed film cooling in front of

the end wall will face the same challenge if a large mass flow and a high cooling momentum are not adopted.

In many studies [26, 30, 59-61], it was aimed to improve the film cooling efficiency and reduce the effect of secondary losses near the wall finish surface, for this purpose, the effect of the geometric contouring of the end wall surface on the end wall inlet leakage flow film cooling was investigated. The findings of these studies show that although there is a noticeable improvement with the contouring of the end wall, this improvement is not significant enough to reduce the required cooling mass flow to acceptable values.

Concerning the flow field and secondary flow models related to the contour profile, Kopper, Milanot and Vancot [62], Boyle and Haas [63], and Moustapha and Willianson [64], presented experimental test results for the contoured endwall surface, which partially explains the reason for the contoured profile development.

There are further researches [65-68] focusing on studies in Leading edge root fillets to control secondary flow losses near the end wall in the hub. In these studies, it has been suggested that by adjusting the fillet shape and size at the leading edge, some degree of compression can be achieved in secondary flows close to the end wall, as well as a reduction in aerodynamic loss. Some studies [69-71] have reported findings on a series of non-axisymmetric endwall contouring. In these studies, it has been suggested that secondary losses and aerodynamic performance can be improved in the hub close to the end wall surface thanks to a non-asymmetric end wall profile.

In their study using the PSP technique, Zhang and Moon [72] compared two axisymmetric platform surface contours, a dolphin nose blade platform shape and shark nose blade platform geometries. They reported that the dolphin nose profile resulted in higher overall

22

film cooling effectiveness, suggesting secondary flows near endwall was better controlled compared to the shark nose geometry. Similar results were also reported by Erickson et al. [73].

In Zhang et al.'s [74] study evaluating three different axisymmetric platform contour designs, Blade platform end wall contouring was found to have a major influence on the flow behavior and temperature distribution near the platform. Similar results were reported by Sangston et al. [75],he suggested in his study that the secondary vortex near the platform and the overall turbine efficiency are significantly affected by the blade root fillet design and contour close to the end platform wall. Li et al. [76] has shown how the film cooling effectiveness and the overall thermal effect of the platform are affected by the "swirl purge flow" at the top of the platform.

Along with the platform contouring, the platform holes and their location have also been shown to affect the flow and thermal distribution on the platform surface, especially at lower blowing rates [77]. It has also been shown that the platform hole contours have a significant effect on the film cooling efficiency, where the contoured holes provide a better film cooling efficiency on the platform surface compared to the basic cylindrical cooling holes [78].

2.3 Rotation Speed Impact on Vane Endwall and Blade Platform Surface Film Cooling Effectiveness

In the study of Ahn et al. [79-81] including rotating turbine experiments, it has been shown that the most critical parameter for the film cooling effectiveness is the turbine rotation speed. The rotation effect is displayed as semi-elliptical shaped dots that spread radially at the design operating speed. Measurements using PSP and findings from systematic experiments show that the angle of incidence changes during an undesigned operation, resulting in a change in the direction of the cooling film. According to the comprehensive studies of Ahn et al. [79-

81], measurements in non-rotating turbine cascades do not cause the above-mentioned model changes.Studies by Suryanarayanan et al. [39, 43] used a three-stage research turbine with two independent cooling cycles, investigating the rotational effects of discharge flow on core platform film cooling effectiveness.. The local film cooling efficiency for upstream stator-rotor cavity injection became better when the rotation speed was increased from 1500 rpm to 2550 rpm. In addition, the efficiency size and dispersion on the platform surface also increased when the upstream injection coolant mass flow rate was increased from 0.5% to 2.00%. Moreover, it was found that the coolant from the upstream slot, affected by the incidence of the inlet flow and the transition vortex, tends to concentrate near the blade suction side of the platform. On the other hand, the discharge flow alone did not provide adequate film protection in the downstream region and across the pressure surface in the rotor platform for the coolant.

Schuepbach et al. [82] and Jenny et al. [83] carried out studies with experimental and computational data on the 1.5-stage high-working axis turbine. Schuepbach et al. [82] investigated the effect of discharge flow on the performance of two different non-axisymmetric end walls contour surfaces. Experimental overall-total efficiency evaluation of the study showed that non-asymmetrical endwalls lose some of their benefit relative to the base case when purge flow is increased. It was observed that the first end wall design lost 50% of the efficiency noted with low suction, while the second end wall design lost 34% [82]. Experimental and computational study of the non-axisymmetric rotor end wall profile in a low-pressure turbine is presented in the study of Jenny et al. [83]. The research findings showed that the measured efficiency revealed a strong sensitivity to the discharge flow of the total-total efficiency. Experiment results revealed an efficiency gap of 1.3% per percent of injected scrubbing flow for the shrouded low-pressure gas turbine configuration with contoured endwalls surface, with an

18% reduction in discharge flow sensitivity due to the endwall profile. Schobeiri and Lu [84] demonstrated the importance of a properly designed end wall contouring in significantly reducing secondary flow losses and thus increasing turbine row efficiency.

In the studies by Suryanarayanan et al. [39, 43] the effect of rotating discharge flow on aerodynamics, performance, and film cooling efficiency of the first stage rotor platform with non-axisymmetric endwall contouring has been focused on.

Similar to the comprehensive review of Schobeiri and Lu's [84] study, there have been a number of recent studies on the effect of wall-end contouring and leading-edge filleting. With the exception of a small number of rotary rig studies on the end wall contouring of Low Pressure (LP) turbines, most of the published work has been performed numerically or experimentally in turbine cascades with constant inlet flow conditions [85-88]. On the other hand, the number of studies on the effect of the end-of-wall contour in rotating turbines is quite low [71, 89-92], as discussed in the study of Schobeiri and Lu [84]. In investigating a cascade, three features are absent: (a) unstable interaction of stator-rotor, (b) platform and blade rotation, and (c) absence of centrifugal forces and their effect on the platform boundary layer. Schobeiri and Lu [84] numerically simulated several cases using the traditional trial and error approach and tried to develop known endwall configurations for application to a rotating rig.

Ahn et al. [81] independently introduced a new physics-based endwall forming method for turbine blades, without applying it to a High Pressure (HP), Intermediate Pressure (IP), or Low Pressure (LP) turbine. This method is based on a continuous diffusion process and uses a predicted slowing of the secondary flow rate from the pressure to the suction surface by a diffuser-type flow path that produces the targeted pressure. The diffuser end wall increases the pressure on the suction side, reducing the secondary flow rate, the power of the secondary

eddies, the associated induced drag forces, and the overall pressure loss from the latter. The steps followed are presented step by step in the related research of Schobeiri and Lu [84]. The method used in the research was applied to the second rotor row of the TPFL turbine and it was seen that it increased the efficiency from 88.82% in the reference state to 89.33% in the newly contoured state. The final efficiency values set forth in the report published by the US Department of Energy [93] show a maximum efficiency of 89.9% for the contoured rotor, while the reference state of non-contoured efficiency t-s is 88.86%. This indicates a 1.04% efficiency increase, almost double the value from the numerical simulation of the 0.51% efficiency found in Schobeiri and Lu's study [84].

In the study of Schobeiri, Lu and Han [94], the effect of end wall contouring as well as discharge flow on the aerodynamics, film cooling and performance of the first row of rotors of a three-stage turbine has been numerically investigated. In related research, it was found that the efficiency gain for the first rotor row was low compared to the second rotor row, as the first row of rotors is directly exposed to the discharge purge flow, resulting in hardware constraints for optimum contouring.

CHAPTER 3

BLADE PLATFORM NON-AXISYMMETRIC CONTOURING IMPACT CONTOURING IMPACT ON SECONDARY LOSSES AND FLOW CHARACTERISTICS NEAR THE HUB

3.1 Objectives

The aim of proposed work is to study contoured platform surface for GP Turbine Blades as a case study we used for this study second stage gas path blade and using ANSYS Adjoint Solver as a surface optimization tool to optimize the secondary flow losses. The first segment of the work is to introduce baseline blade contour, the optimization study objectives and boundary conditions of main and purged cooling flow. The objectives of this segment of the study are to optimize for blade contour that will achieve the lowest pressure ratios between pressure and suction sides of the platform to minimize cross flow which increases losses. As we discussed earlier horse-shoe vortex that develop between two adjacent blades near platform has a negative impact on efficiency, power and film cooling effectiveness which impacts platform temperature, on this study we will focus on evaluating film cooling effectives for three different platform contour shapes for second stage GP blade which will be compared to baseline conventional blade platform contour. The first segment of the work will be Computation Fluid Dynamics (CFD) optimization using adjoint solver tool technique in ANSYS to minimize pressure ratio and limit flow between suction side and pressure side near blade platform, the aim of this study is to come up with several contours proposals for experimental validation that will provide 5%, 10% and 20% reduction in average pressure difference between blade suction side and pressure side near platform surface.

The second segment of the work will be a CFD model validations for all the three contours with updated platform contour mesh and applying the closest to reality engine operation conditions and compare with the optimizer suggested pressure reduction percent value and compare with baseline approach.

3.2 Scope of Work

Initially started with the existing second stage turbine blade baseline platform contour configuration to get a start point on how the current behavior of contour shape on cooling efficiency, vortex and flow efficiency near platform wall. Second step was running adjoint solver optimizer and set optimization objectives and parameters in order to modify the platform contoured for 5%, 10%, and 20% pressure delta reduction between PS and SS near the hub.
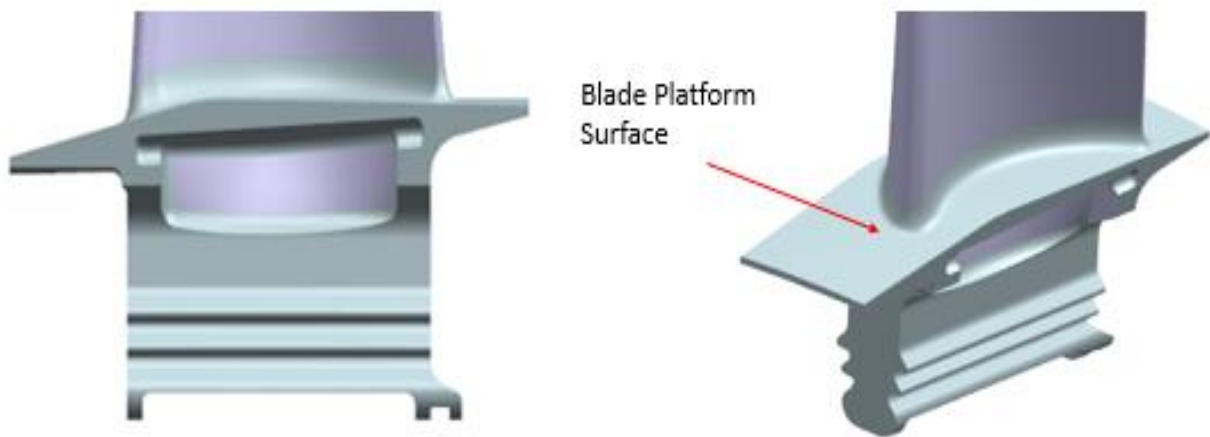
Figure 17 Baseline Second Stage Blade Flat Platform

3.3 GP Second Stage Blade Overview
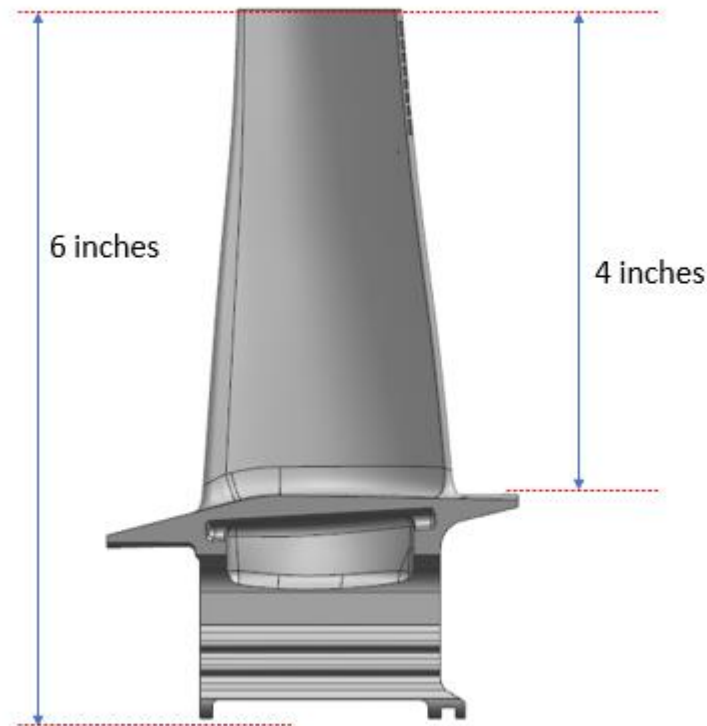
Figure 18 GP Stage 2 Blade General Dimensions

The overall length of the used in study second stage GP blade used in the study is approximately 6 inches in total height and the aerofoil is approximately 4 inches in height. The engine has 70 blades in the second stage that is fixed in a rotor disk. The blade is casted with a nickel-based alloy that is most resistant to creep and fatigue damage.

3.4 Linear Cascade Overview

A five-bladed linear cascade was used in the study. The overall dimensions for the main-stream flow entrance opening is approximately 18 inches wide and 5 inches high. the main-stream flow outlet opening is approximately 12 inches wide and 5 inches high as shown in the below in Fig 19.

a)   b)

Figure 19 a) Linear Cascade Test Rig Main Flow Inlet Opening Dimensions, b) Linear Cascade
Testy Rig Main Flow Outlet Opening Dimensions

Figure 20 Linear Cascade General Dimensions
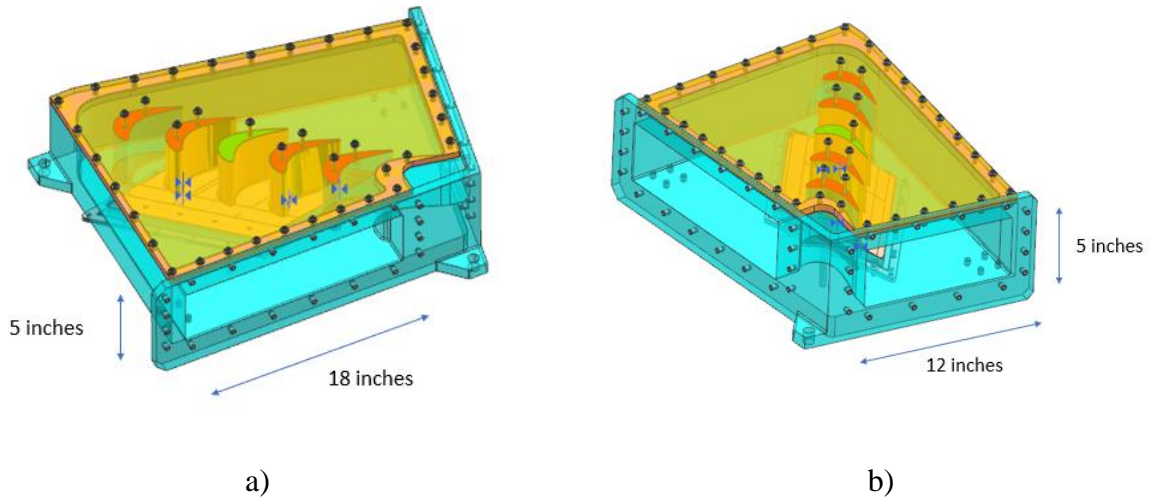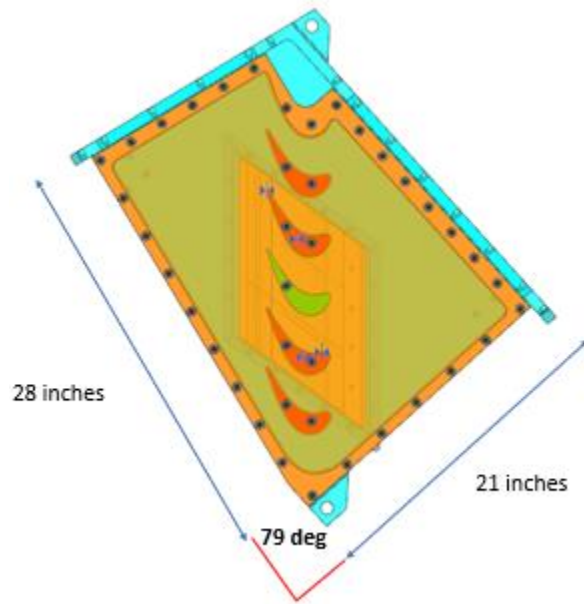
The flow rotates almost 79 degrees after passing through the 5 blade assemblies

providing almost 6 blade passages as shown in Fig 20.

3.5   Setup CFD Model for Second Stage GP Blade Baseline Blade Platform Fluid Domain

 and Identify Required B.Cs

First segment, design the baseline platform for second stage blade used in the study

without contour just with a baseline flat surface and generate fluid domain that is inspected

precisely for any faults having main-stream for the cascade extended and having bleed air inlet

parallel to the platform front end. The mesh technique used in the model was done using

adaptive mesh with the first and second derivative of pressure as adaption switches for the mesh.

Engine boundary conditions that is most close to reality were applied, next identified

optimization objectives to minimize delta pressure at platform/blade intersection between PS

(pressure side) and SS (suction side), used 5%, 10%, and 20% as delta pressure reduction targets.

In this study the optimization observable used is the average pressure difference between Suction

Side and Pressure Side near the platform hub.

The second part was mainly focused on validating generated platform contours to verify

pressure difference value reduction and compare pressure distribution near the platform surface

with the baseline model and determine how close the optimizer predictions to actual analysis

values after modified top of the platform mesh with updated contour geometry.

3.6   Future Work Experimental Validation using Linear Cascade for Baseline Platform

 Contoured Geometry

This will be used for future work that is not included in this research study, where 3D

printed platform surfaces with three proposed platform configurations generated from the

optimization study on this study using Adjoint Solver and setup the test rig to validate data with

real experimental data.
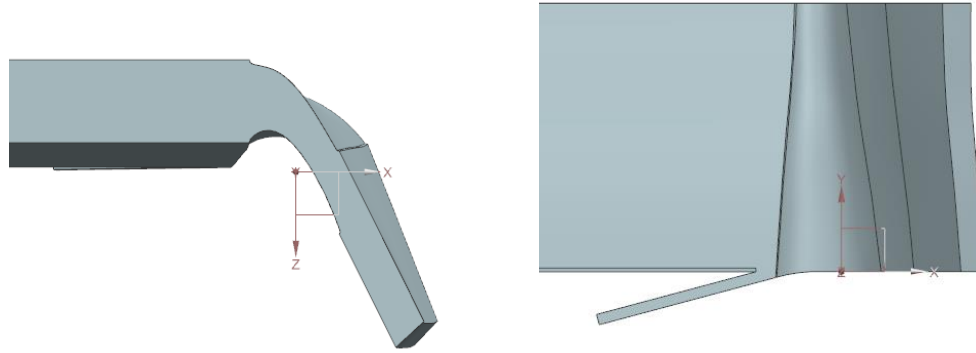
Figure 21 Sector Flow Domain for Mainstream and Purge Flow

3.7 Methodology
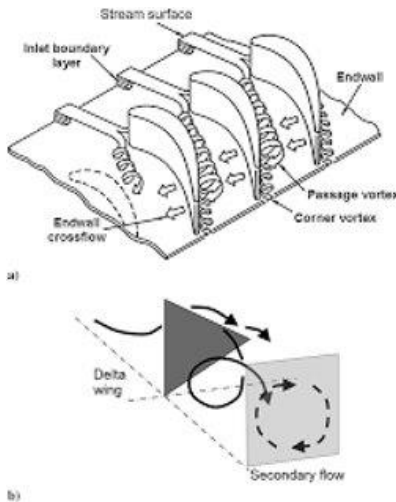
Figure 22 Near Platform Vortex [95]

3.7.1   New Modified Blade Platform Film Cooling Optimization Design Features

Design updated geometry using adjoint solver tool built in ANSYS fluent, platform surface was segmented into tiny segments and applied geometrical bounds and envelop to move and change shape depending on a set target with applied B.Cs as explained in the following sections.

Geometry has been extracted to match the linear cascade test rig where linear sector model used between pressure and suction side of the middle blade in the linear cascade as shown in the Figure 23.

Figure 23 Linear Cascade Test Rig Assembly

Figure 24 Mainstream Fluid Domain Linear Sector
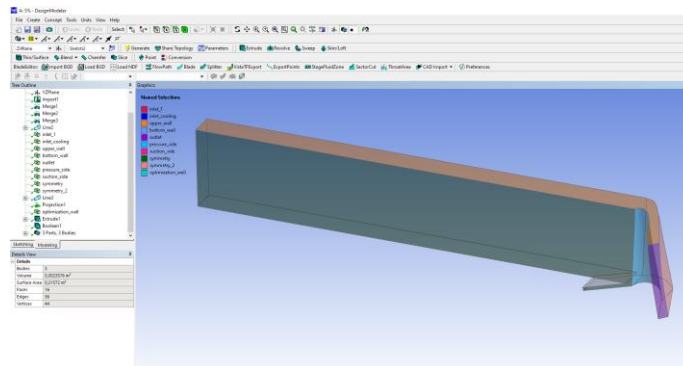
Figure 25 Mainstream Fluid Domain and Purge Flow Bleed

As show in Fig 25 main-stream flow was modeled with mass flow rate and pressure B.Cs using air total temperature, total pressure, Mach number and mass flow rate for inlet and outlet as shown in Table 2. Purge bleed flow has been modeled with mass flow rate and purge flow inlet total pr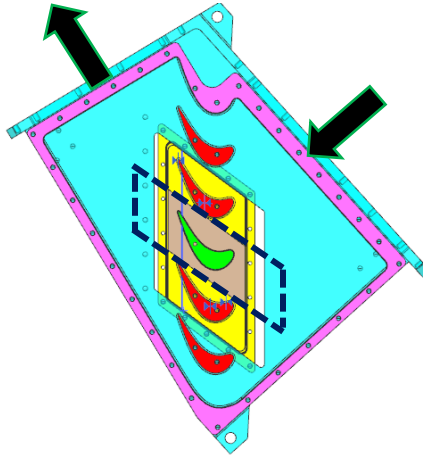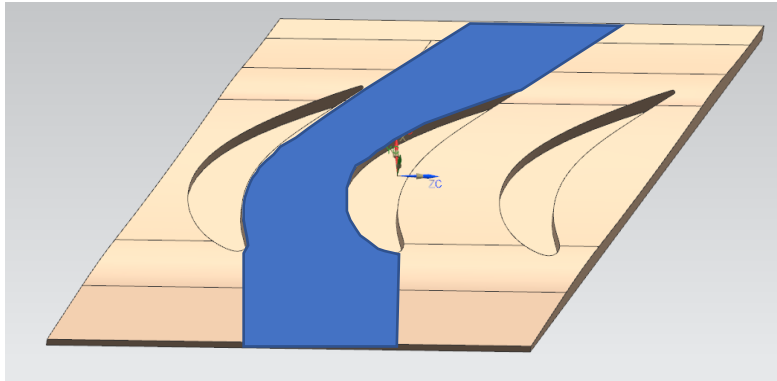essure per Table 3, the purge bleed flow merges with main-stream flow at the front segment of the platform before blade leading edge.

Model mesh controls has been applied to capture as accurate as possible velocity and pressure gradient near walls using adaptive mesh technique.
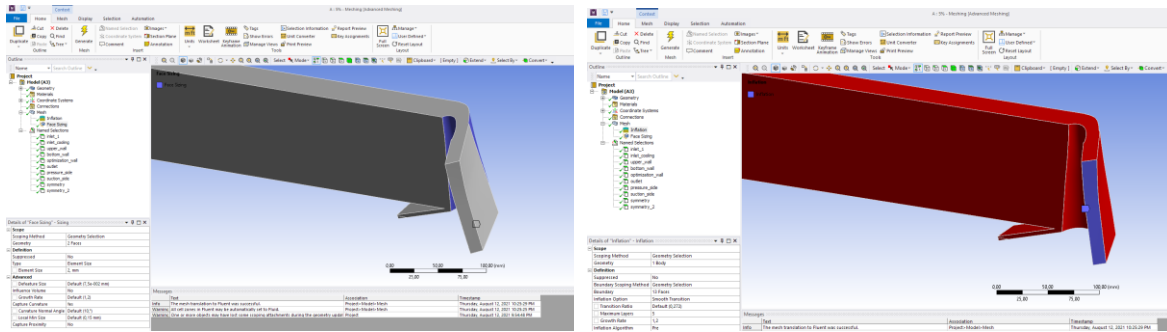
Figure 26 Face Mesh Wall Mesh Control

3.7.2 Fluent CFD Model Setup

Ansys Fluent was used to create and solve the CFD model with applied B.Cs to estimate the pressure distribution near the platform hub, in addition to Adjoint Solver for platform contouring optimization.

3.7.3 Adjoint Model Setup

Adjoint Solver settings has been used as shown in the Figure 27 where platform surface has been identified and geometrical bounds with X, Y, Z has been identified in order to give freedom for the surface mesh to stretch to the best shape that will fulfill the optimization objective.

Optimization objectives has been identified as ΔP the difference between PS & SS near the platform wall, and the optimization were performed for the three cases, ΔP value decrease with values 5%, 10%, and 15% reduction in pressure difference.
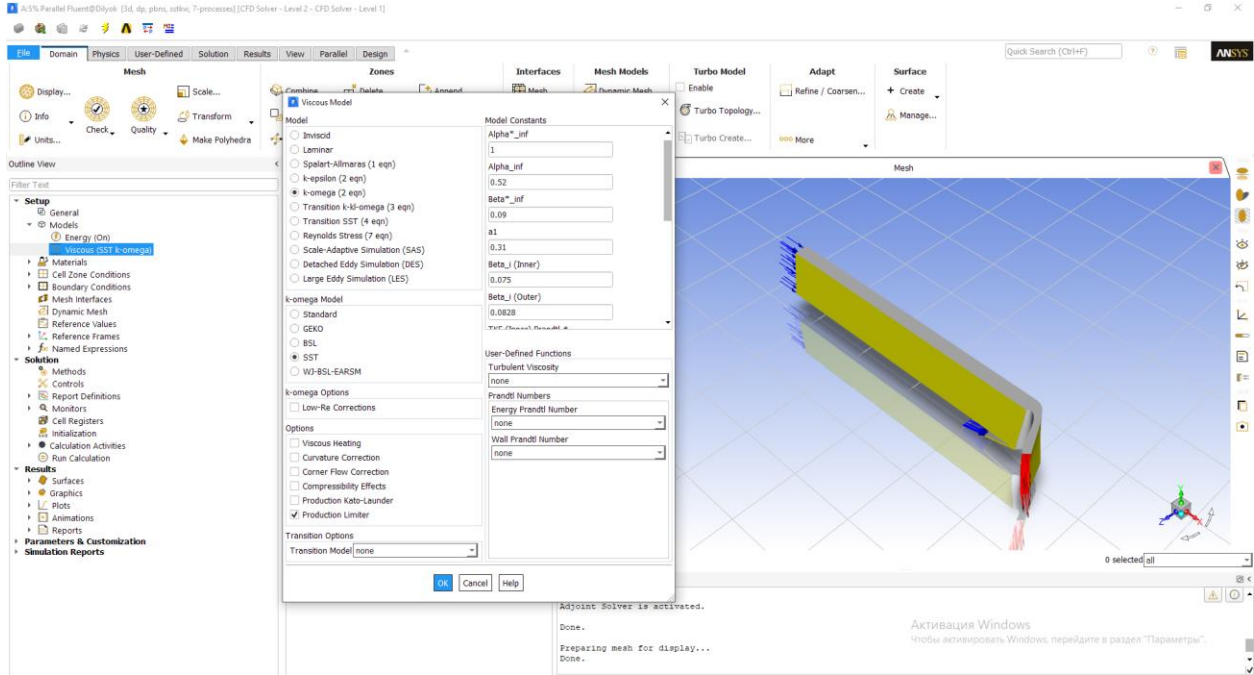
Figure 27 Adjoint Solver Settings

3.8   Boundary Conditions

Main-stream flow was modeled with closest to real engine application and similar to the linear cascade setup that will be used in the future work, ,where mass flow rate were estimated to be 0.481 kg/s per segment (used two segments) with total mass flow rate 0.96 kg/s. Total pressure, total temperature and Mach number values were chosen to be closest to the linear cascade test rig setup, purge bleed flow was also modeled with air MRT (Mass Flow Rate) of 0.0048 kg/s (0.5% of main-stream) per passage segment.

Mach number at inlet was also specified to 0.635. Wall condition was applied to all

surfaces and walls. Platform bleed mass flow rate was applied to replicate the bleed flow on the

real engine operation that can perform as a film to protect the platform from overheating.

3.9   Fluid Domain

Fluid Domain has been identified with 2 between blade passage segments to avoid

extracting data on the boundary and have a continuous flow for uniform passage.

Figure 28 Linear Cascade
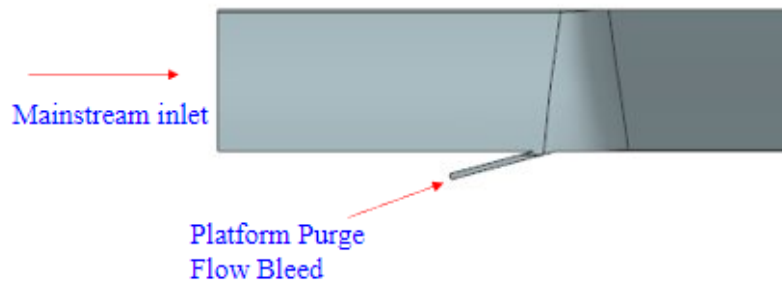
Figure 29 Mainstream and Purge Flow
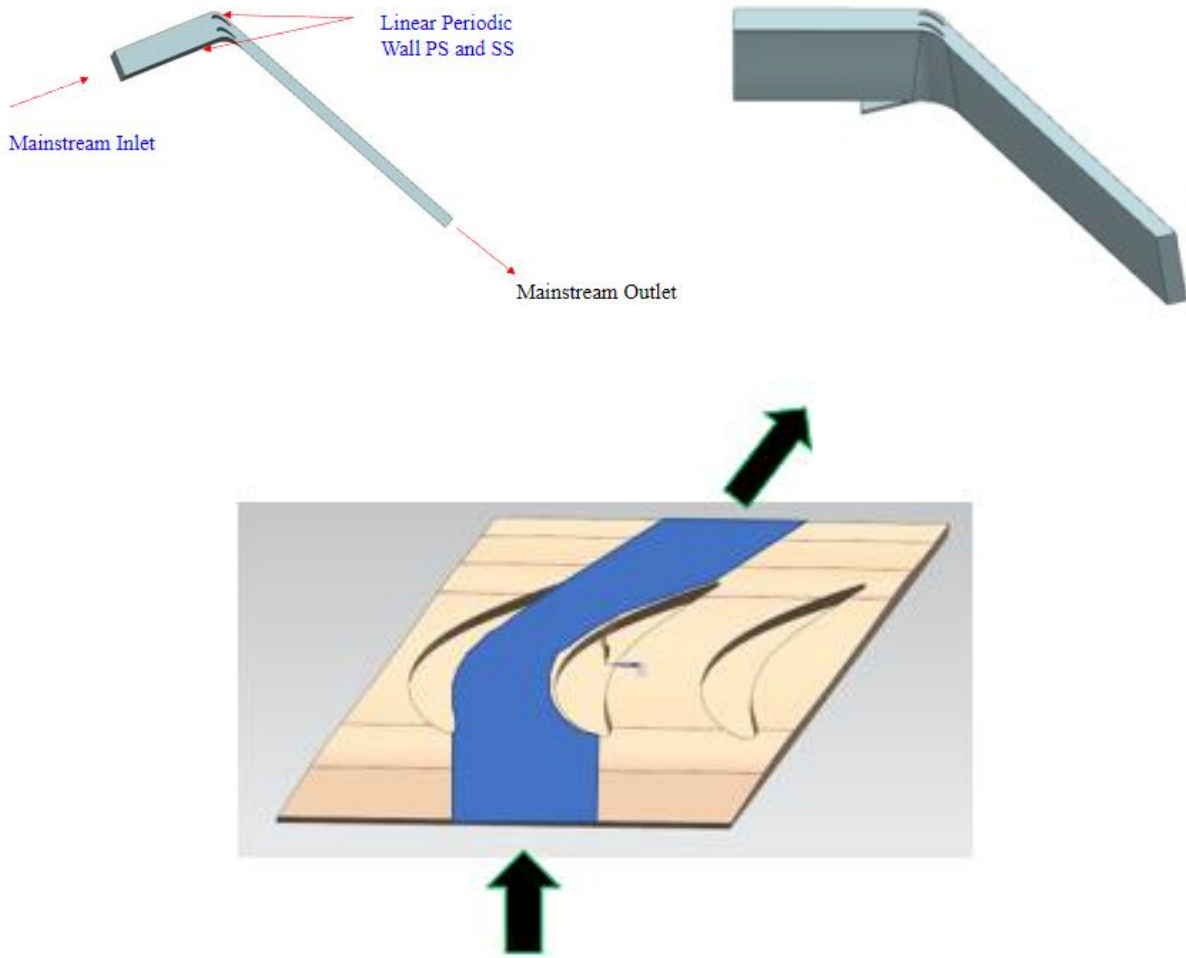
Figure 30 Platform Surface on Linear Cascade

Platform surface was segmented into tiny segments and will apply geometrical bounds and envelop to move and change shape depending on a set target and B.Cs as explained in the following.

3.10 Boundary Conditions for Mainstream and Purge Flow

Table 2 Main Flow Conditions

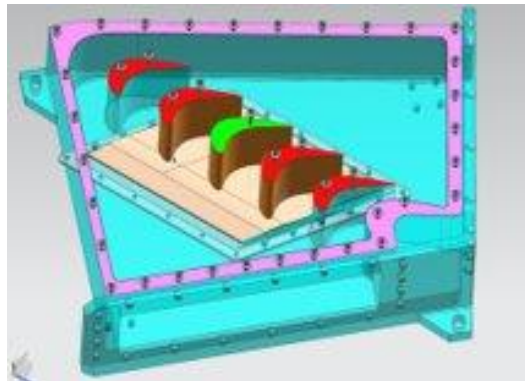| Main Flow Conditions		
m, Kg/s	P_{1t}, Pa	Tt, Kelvin
0.96	92503.37	973

Table 3 Bleed Flow Conditions

Bleed Flow Conditions		
m, Kg/s	P_{1t}, Pa	Tt, Kelvin
0.0048	92503.37	486.5

As previously explained main-stream flow was modeled with mass flow rate 0.481 kg/s per segment (used 2 segments for convergence) and total pressure applied is 92503.37 Pa, inlet main-stream air total temperature was set to 973 Kelvin that has been calculated based on isentropic flow conditions shown on Equation 1, Purge feed flow has been modeled with Air mass flow rate of 0.0048 kg/s (0.5% of main-stream) per 2 passage segment and total inlet purge temperature was set to 486.5 Kelvin, and total pressure value of 92503.37 Pa, which also calculated using isentropic flow conditions on Equation 1, Mach number at inlet was also set to 0.635.

$$\frac{T_t}{T} = 1 + \frac{\gamma - 1}{2} * M^2 \qquad\qquad \frac{P}{P_t} = (1 + \frac{\gamma - 1}{2} * M^2)^{\frac{-\gamma}{\gamma - 1}}$$

Equation 1 Isentropic Flow Total Pressure and Total Temp Equation

Linear periodic wall B.Cs was set on the PS and SS of the fluid domain, Wall B.Cs was set for the top and bottom plate of the linear cascade, inlet extended to 5 times chord length and exit was extended to 15 times chord length for most accurate results.
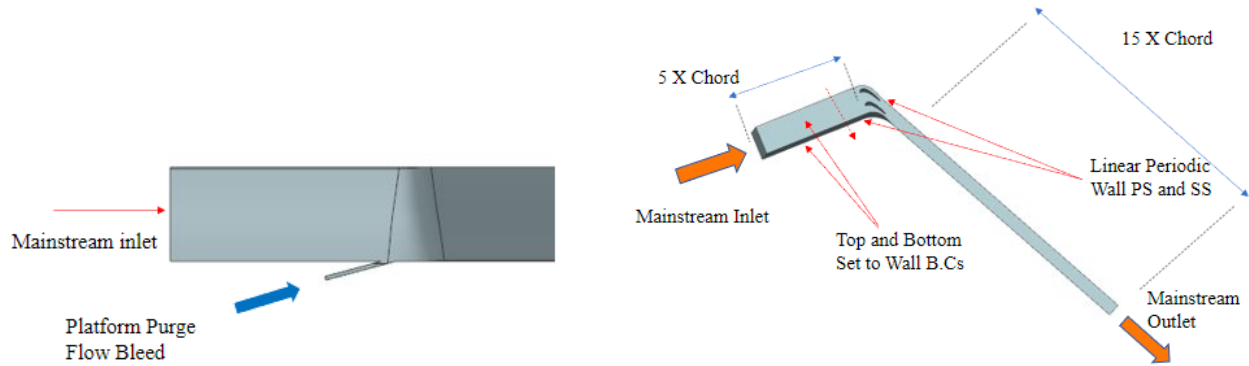
Figure 31 B.Cs, Inlet, Outlet and Bleed

The Fluent model was coupled with an adjoint solver to optimize for surface geometry, where we applied target observables (optimization function), in this case we used optimization observable ΔP (Delta Pressure) as an observable where:

$$\Delta P = P_{average\ pressure\ on\ pressure\ side\ near\ hub} - P_{average\ pressure\ on\ suction\ side\ nea\ hub}$$

Equation 2 Delta Pressure Observable Function Used for Optimization
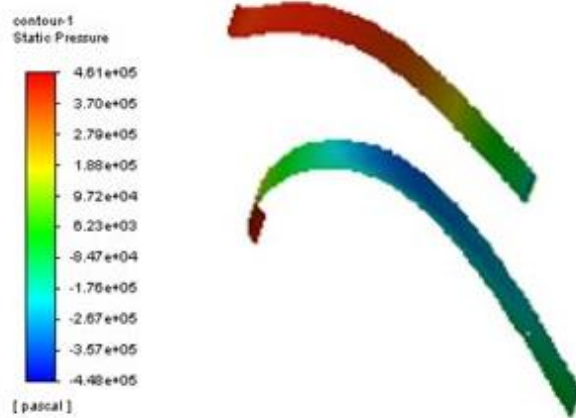
Figure 32 Near Platform PS and SS Pressure Contours Baseline

3.11 Mesh

Initially the mesh has 769512 elements, 3 IL (Inflation Layers) are used next to the walls. The mesh was adapted during the solution to better resolve the flow features, resulting in a mesh with 2334773 elements mix tetrahedral, hexahedron and pentahedron elements.
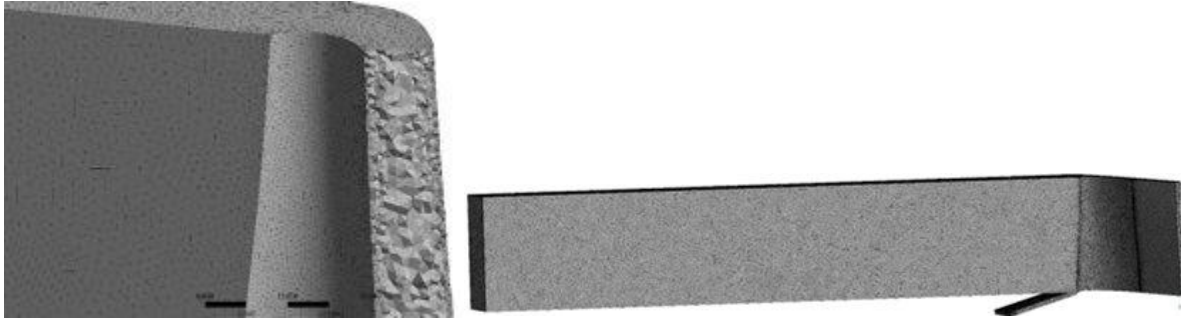
Figure 33 Fluid Domain Mesh Images
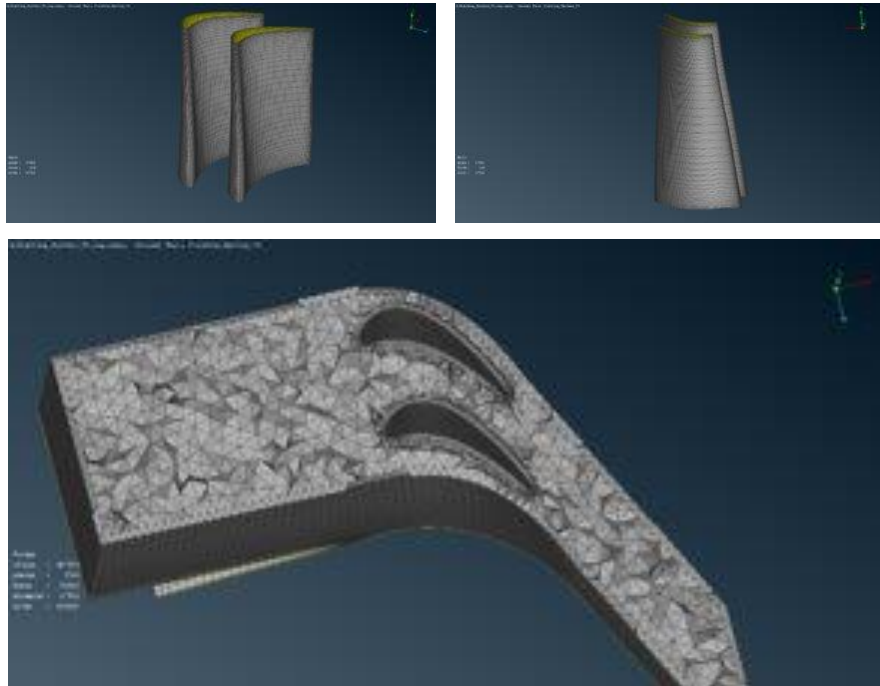
Figure 34 Fluid Domain Blade and Boundary Layers Mesh Quality Images
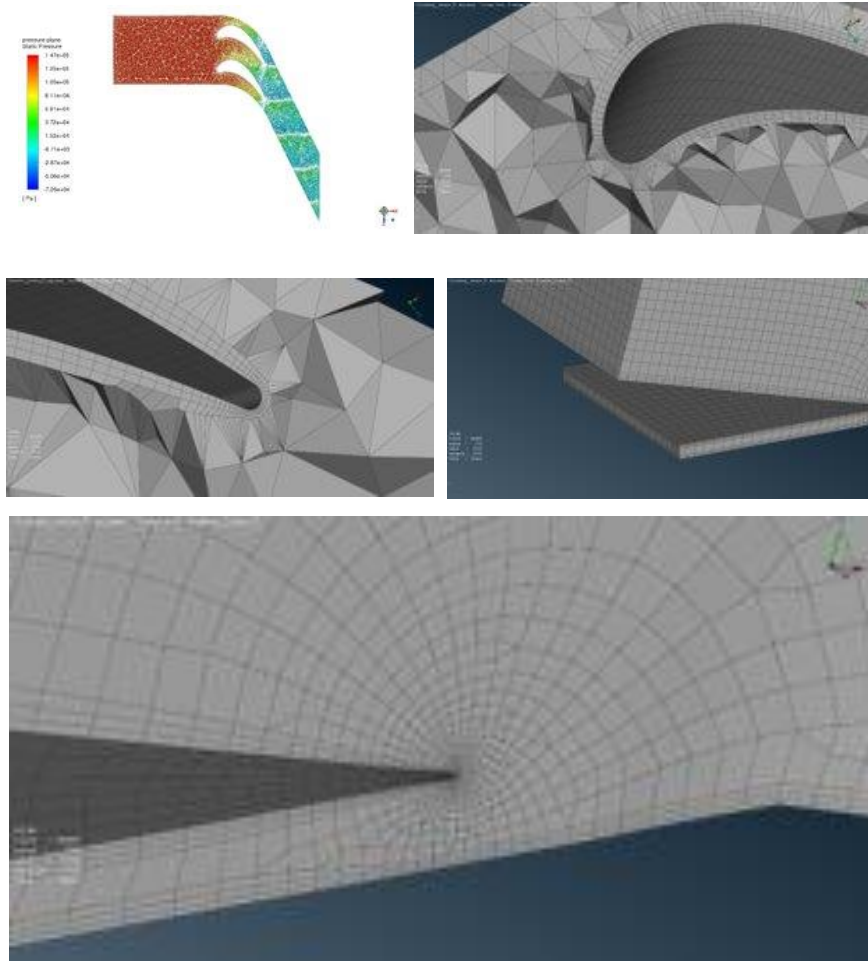
Figure 35 Fluid Domain Blade and Boundary Layers Mesh Quality Images with Blade Purge Flow and Aerofoil

3.12 CFD Model Setup

Pressure-based coupled solver and energy equation, Ideal gas, Sutherland's law for viscosity, Kinetic theory for specific heat and thermal conductivity.

Adaptive mesh with the first and second derivative of pressure as adaption switches for the mesh.

Pseudo-transient formulation for the solution, Steady state conditions and k-ω SST model for turbulence model setup used.

We also setup a geometrical bound as shown in the Figure 36 for the platform that allows mesh to adjust and extend radially within these bounds.

Specified mass flow inlet for the blade passage, specified mass flow inlet for the purge flow, define mass flow rate, total pressure and total temperature at inlet, pressure outlet at the exit (atmospheric pressure), periodic boundaries at the sides of the flow passage, adiabatic flow conditions at all walls have been used.
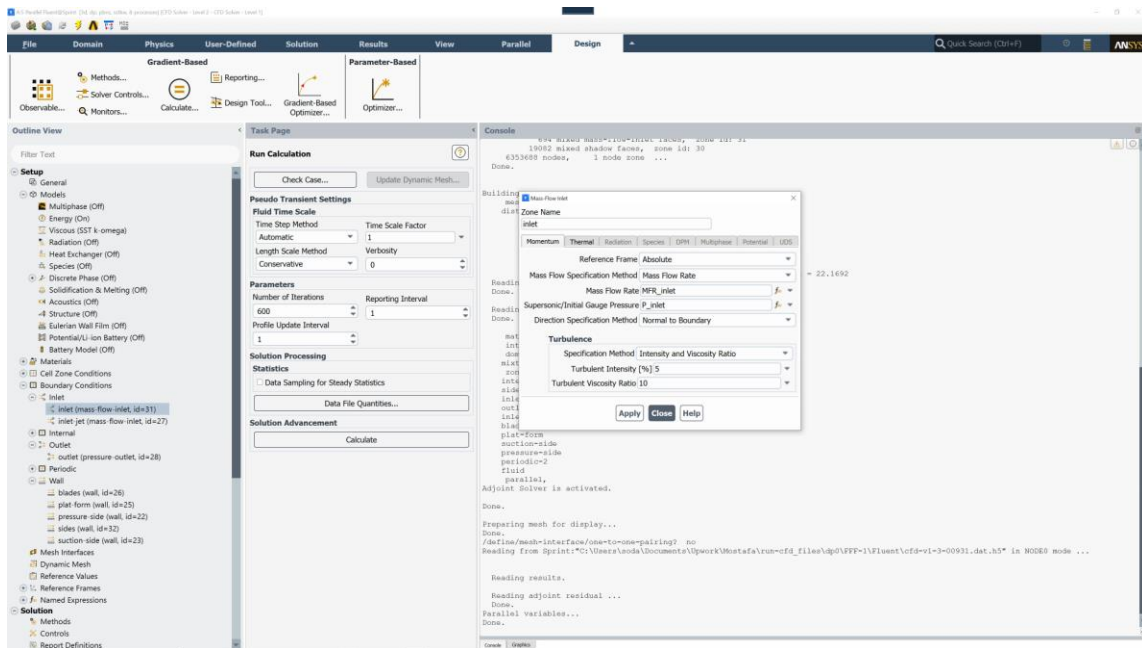
Figure 36 ANSYS Fluent B.Cs
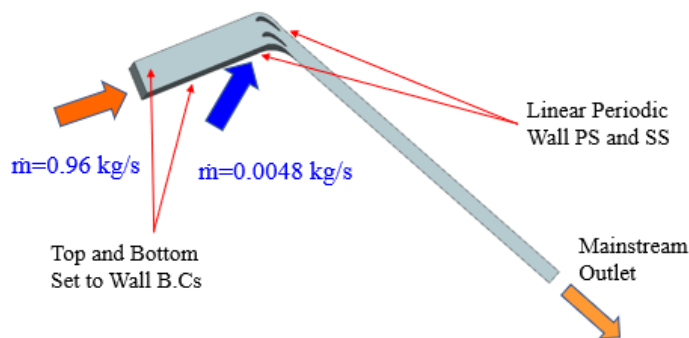
Figure 37 Main Stream and Purge Flow B.Cs

3.13 CFD Model Postprocessing and Results
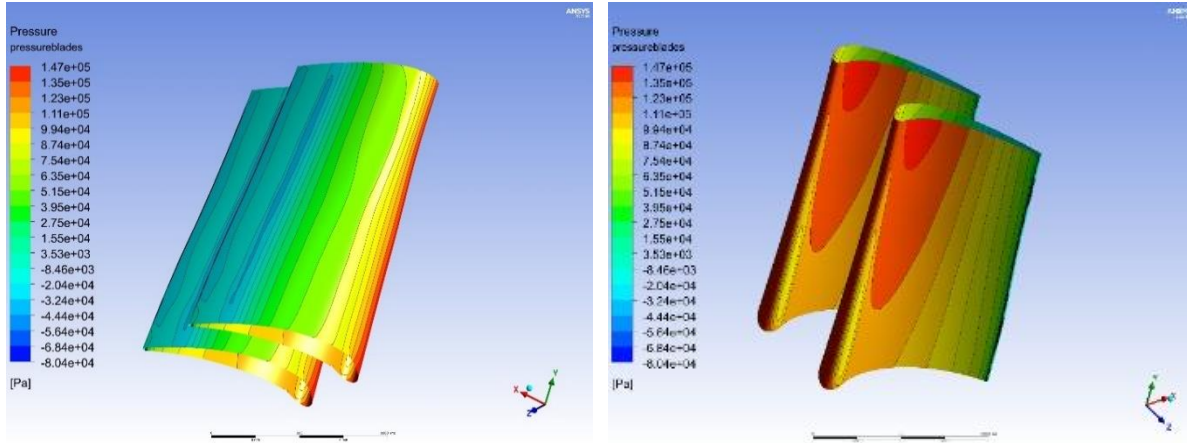
Figure 38 Aerofoil PS and SS Pressure Distribution

3.14 Mach Number Comparison
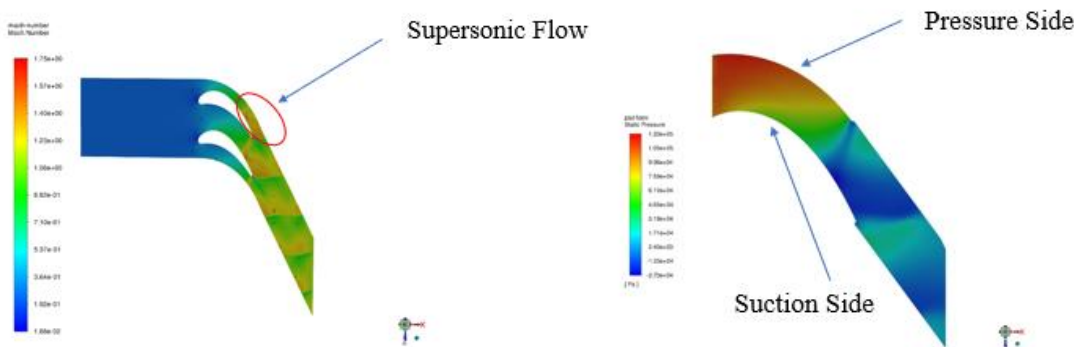
Figure 39 Mach Number Distribution for the Blade Passage

Inlet flow as showing in Fig 39 is subsonic as flow enter the passage between the blades it increases its velocity specially at SS and gets supersonic.

Pressure gradient near platform has been noted between PS and SS edges with the blade near the hub.

Observable used in the study is area weighted pressure on the suction side and pressure side near the hub. Where $\Delta P = P$ (Pressure Side) $- P$ (Suction Side), First order (for convergence

reasons), applied Adjoint Energy and Ideal Gas activated, Adjoint solver shown ΔP (initial)

estimated to be 54822.297 Pa.
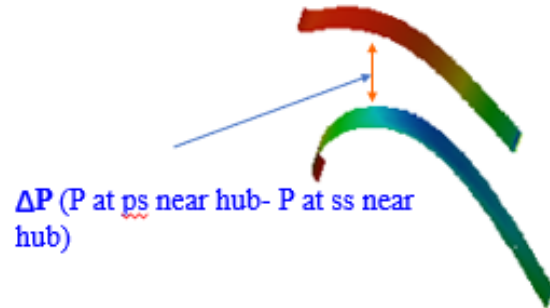
Figure 40 Near Hub PS & SS Delta P
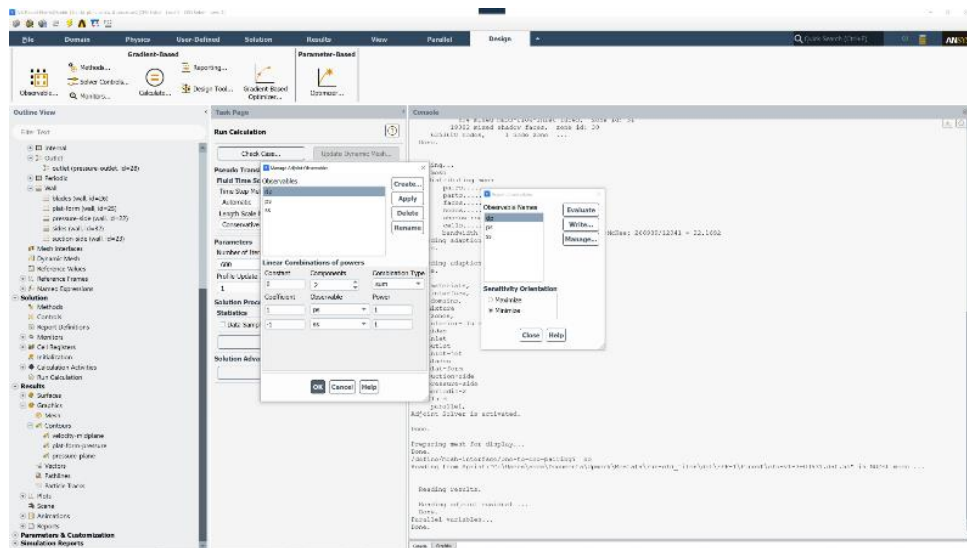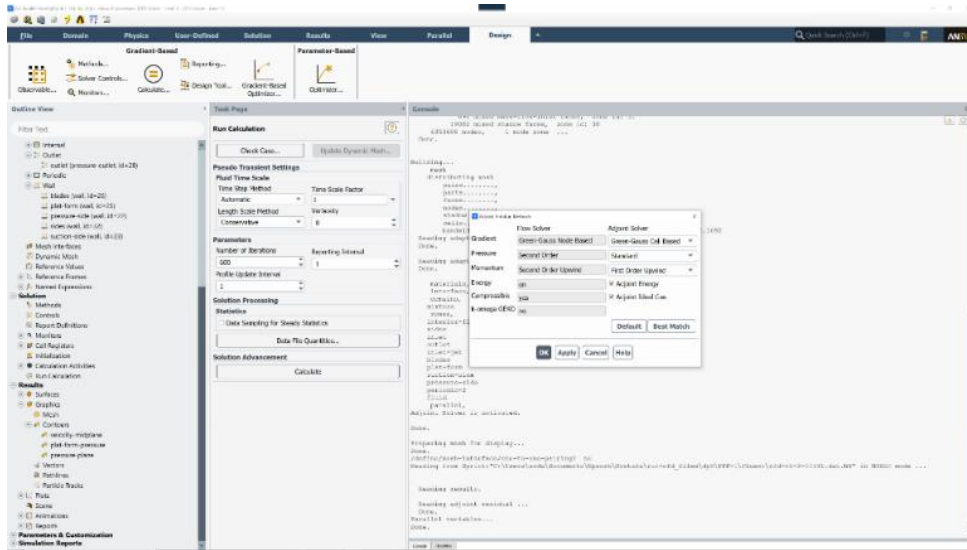
Figure 41 Observables at Adjoint Solver Optimization Tool
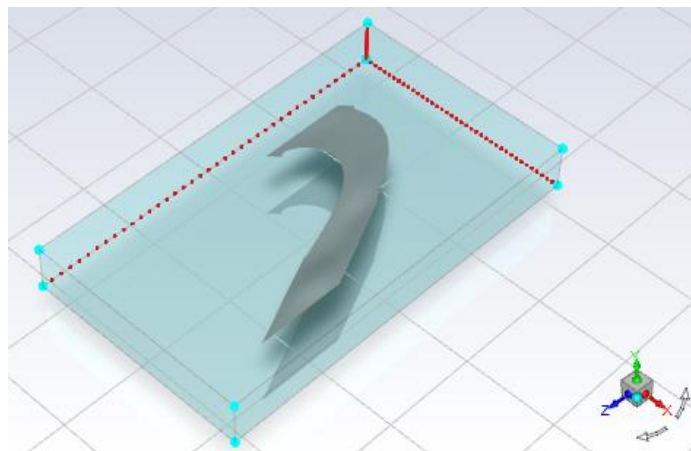
Figure 42 Mesh Change Envelope on Platform

The targeted delta pressure reduction values of 5%, 10%, and 20% reduction between PS and SS near the hub was set, mesh modified after each optimization run within the geometrical boundaries that we set in the Adjoint Solver, Non-symmetric changes applied to platform surface mesh, modified mesh then exported to a cad contour surface for further evaluation.

3.15 Platform Contour (Case A) 5% Reduction in ΔP

Figure 43 Top and Side View for Platform Surface at 5% Delta Pressure Decrease (Case A)
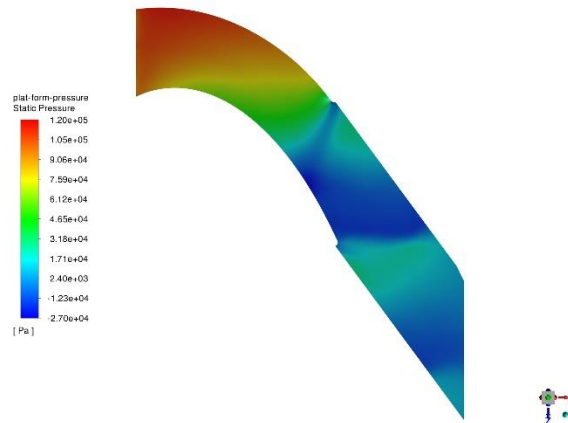
Figure 44 Static Pressure at Platform Surface with 5% Delta Pressure Decrease

It can be noticed a non-axisymmetric contour change to the surface of the platform in the AFT side of the platform, pressure difference near the hub between PS and SS is initially estimated by the adjoint solver to be ΔP (initial) of 54822.297 Pa for the baseline model.

With applying 5% reduction in ΔP to minimize circumferential flow component form PS to SS near the hub, the 5% ΔP decreased case A was showing ΔP reduction value estimated by the optimizer to be 2741.078 Pa between PS and SS.

The change on the platform surface profile was shown on the -Y direction maximum value of 0.0118″ was localized on the PS TE side and on the +Y direction maximum value of 0.004″ at passage exit section.

The updated platform surface profile was incorporated in the 3D CAD model. A new CFD study was performed with baseline-similar settings and B.Cs to evaluate the change in ΔP value with modified platform with 5% reduction in ΔP.

The ΔP value reported on the validation model for platform contour on case A has calculated to be an actual value of 52113.664 Pa, which makes the calculated reduction in the actual CFD validation model is around 2708.633 Pa, that is calculated to be 4.94% reduction in ΔP compared with the baseline initial ΔP value of 54822.297 Pa.

The reported results appear to agree with the initial estimate with an error of about 0.06% with Adjoint Solver optimizer initial predictions.
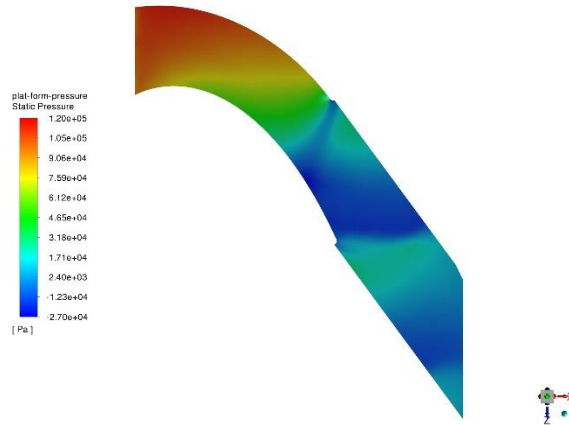
Figure 45 Case A Platform Pressure Distribution for the Validation Model with 5% ΔP Reduction

As shown in Fig 44, the pressure distribution for the actual CFD validation model is in agreement with the optimizer initial predictions pressure distribution over the platform surface.

3.16 Platform Contour (Case B) 10% Reduction in ΔP

It can be noticed a non-axisymmetric contour change to the surface of the platform in the AFT side of the platform, pressure difference near the hub between PS and SS is initially estimated by the Adjoint Solver to be ΔP (initial) value of 54822.297 Pa.

Additional 5% reduction in ΔP applied to case A model aiming for minimizing circumferential flow component from PS to SS, for 10% ΔP decrease, the ΔP reduction value was estimated by the optimizer to be 5482.111 Pa.

Further modification has been noticed on the passage at TE section compared with case A contour profile on the labeled area in Fig 46, between the pressure side and suction side a stretch on the platform surface in the –Y direction in the amount of 0.025" was measured, and the area at the TE Suction Side showed modified platform surface on the +Y direction with the amount of 0.016" as shown in Fig 46.
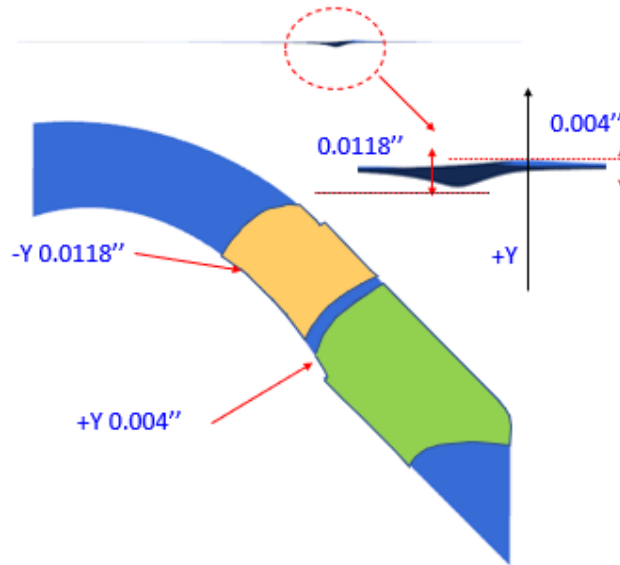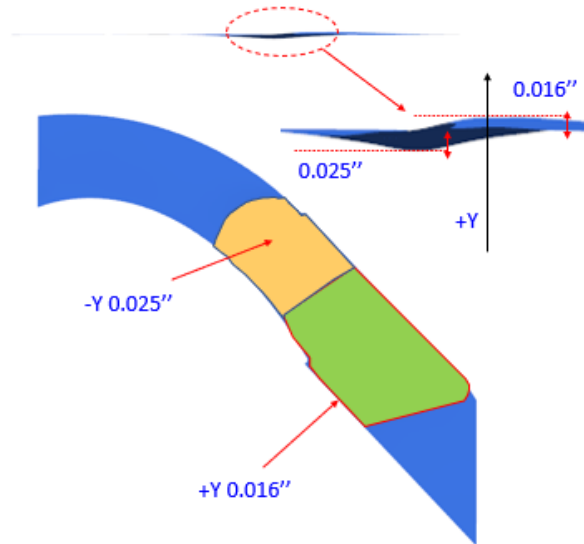
Figure 46 Top and Side View for Platform Surface at 10% Delta Pressure Decrease (Case B)
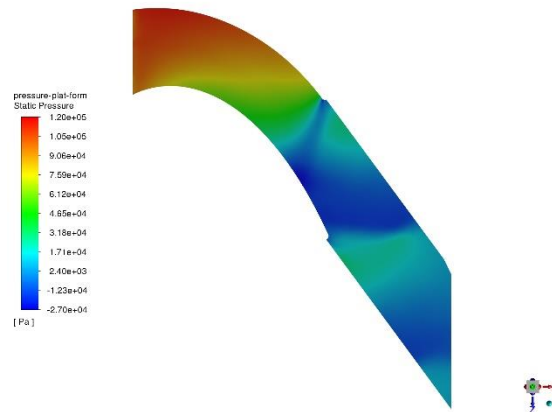
Figure 47 Static Pressure at Platform Surface with 10% Delta Pressure Decrease (Case B)

The updated platform mesh has been modified on the 3D Cad model similar to the changes done on case A study to reflect the changes on the platform with 10% reduction in pressure difference, new CFD run with similar settings and B.Cs to the baseline has been applied to evaluate the change in the ΔP value and validate it with the optimizer initial ΔP predictions.

The ΔP value reported on the validation model for platform contour on case B was calculated to be actual value of 49021.449 Pa, the calculated reduction in the actual CFD

validation model is calculated to be 5800.84 Pa, that is calculated to be around 10.58% reduction

in ΔP compared against the baseline model of initial run with total ΔP value of 54822.297 Pa.

Reported results is in agreement with the initial estimate with a calculated error of 0.58%.
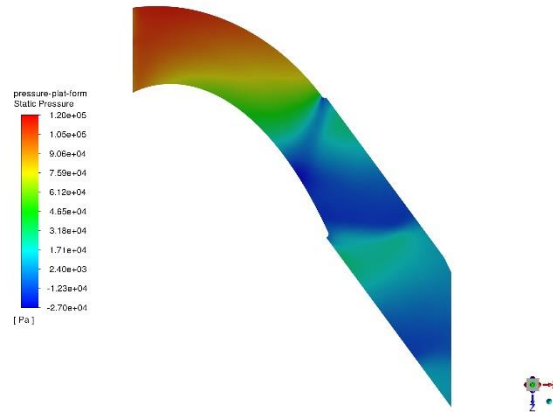
Figure 48 Case B Platform Pressure Distribution for the Validation Model with 10% ΔP
Reduction

3.17 Platform Contour (Case C) 10% Reduction in ΔP

Similar to case A and case B models, it has been noticed a non-axisymmetric contour

change to the surface of the platform in the AFT side of the platform in case C, as previously

reported in case A and case B pressure difference near the hub between PS and SS is initially

estimated by the adjoint solver to be ΔP (initial) value of 54822.297 Pa.

Applied 20% total reduction in ΔP in order to minimize circumferential flow component

form PS to SS, for 20% ΔP decrease, the total ΔP reduction value was estimated by the optimizer

to be 10964.15 Pa.

Even more noticeable modification took place on the passage TE section as shown on the

labeled area in Fig 49 between the pressure side and suction side in the –Y direction with the

amount of 0.061″ and the area at the TE Suction side got modified on the +Y direction with the

amount of 0.040″.
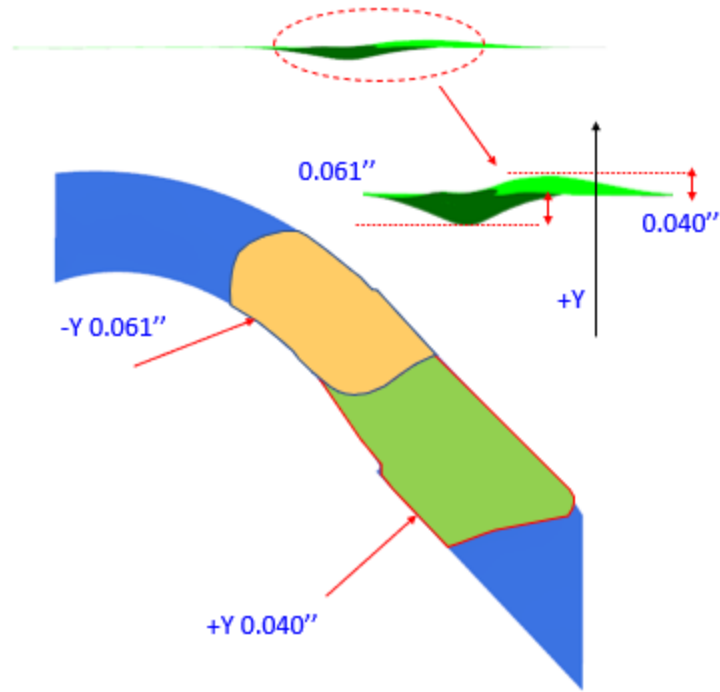
Figure 49 Top and Side View for Platform Surface at 20% Delta Pressure Decrease (Case C)
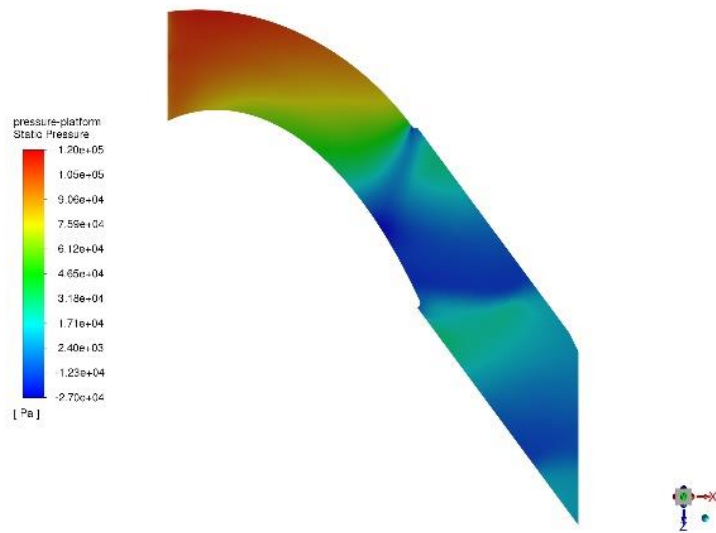
Figure 50 Static Pressure at Platform Surface with 20% Delta Pressure Decrease (Case C)

The updated platform mesh has been modified and updated in the 3D model with updated platform contour for case C, and a new CFD run with similar settings to the baseline has been run to evaluate the change in the ΔP value.

The ΔP value reported on the validation model for platform contour on case C was calculated to be an actual value of ΔP reduction in amount of 11560.965 Pa with total ΔP of 43261.332 Pa, that is calculated to be 21.08% reduction in ΔP using the baseline value of initial run ΔP=54822.297 Pa.

The results appear to agree with the initial Adjoint Solver optimizer estimate with an error of about 1.08%.
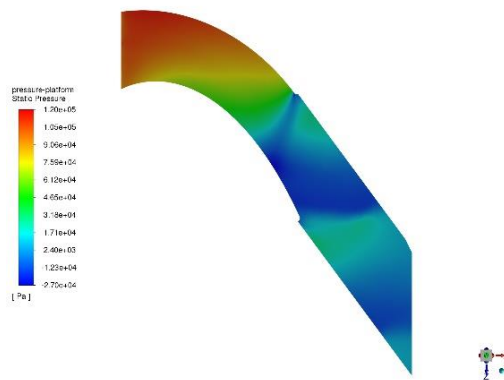
Figure 51 Case C Platform Pressure Distribution for the Validation Model with 20% ΔP Reduction
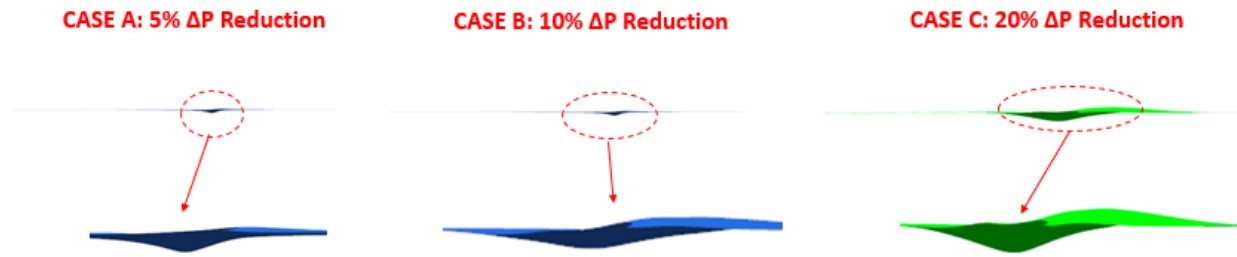
Figure 52 Summary for Optimized Platform Surface for the Three Cases with 5%,10% & 20% ΔP reduction

The highest-pressure reduction in the amount of 20% was shown in case C modified platform surface results shows a larger change for the platform contour compared to case A and case B. It was also noticed that the front end of the platform is not sensitive to the pressure gradient value near the hub, on the other hand the platform Aft exit section is more sensitive to the pressure gradient between PS and SS edges near the hub, the changes on the platform was taking effect starting from roughly 50% Chord and extended to the exit section.

Baseline

Case A: 5% Reduction

Case B: 10% Reduction
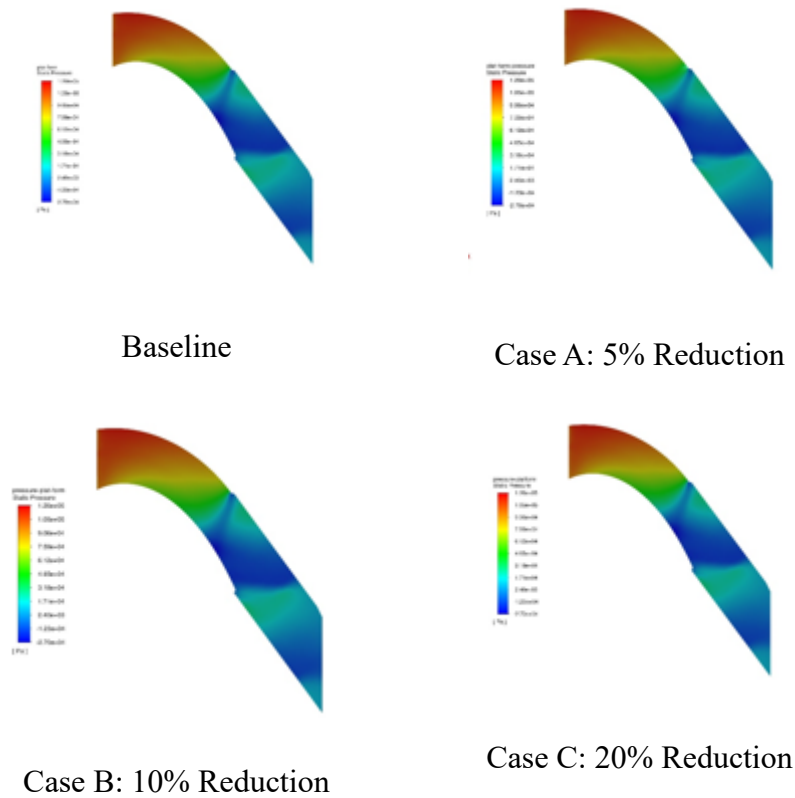
Case C: 20% Reduction

Figure 53 Pressure Patterns for the Three Cases with 5%,10% & 20% ΔP reduction

Visually the pressure pattern appears the same near the platform, the highest reduction in ΔP value was noted in case C with 20% reduction that reflect a total ΔP value of 43261.332 Pa.

Model has been validated using the three different platform contours applied, pressure delta reduction reported for 5%, 10%, 20% respectively for the three platform contours was matching the ΔP value reported using the adjoint solver predictions.

CHAPTER 4

CONCLUSION AND RESULTS

4.1 Conclusion and Results Overview

The highest ΔP value reduction was noted at case C 20% reduction with total ΔP value of 43261.332 Pa. The highest-pressure reduction with 20% in case C shows the most change happened on the platform surface. It was also noted that the front end of the platform surface contour is not sensitive to the pressure gradient between PS and SS near the hub.

It was discovered that the Platform Aft section surface contour is more sensitive to the pressure gradient between PS and SS edges near the hub. The changes on the platform were taking effect starting from roughly 50% chord length and extend to the exit by ¼ chord length.

Verification runs for case A blade platform contour were performed with updated mesh settings and mesh density to reflect the changes on the platform top surface and it was found that it is in agreement with the Adjoint Solver optimizer initial predictions, the same process has been repeated for case B and case C blade platform contour and both were also showing consistency with results that was predicted with the Adjoint Solver optimizer with a small error percentage in the ΔP anticipated reduction.

Fig 52 showing the detailed changes on the three contours for the three different blade platform contour configurations 5%, 10%, and 20% percent reduction, contours were exported to CAD to reflect the changes on the blade geometry.

In case C for the 20% pressure difference reduction, we have noticed an increase in the surface non-axisymmetric changes and modification on the passage of the TE section as showing in the labeled area on Fig 46 between the pressure side and suction side in the –Y direction by 0.061″ and the area at the TE Suction side stretched the surface in +Y direction by 0.040″.

Secondary losses have a great impact on GP performance and blade platform temperature near platform vortex which impacts blade platform film cooling effectiveness and overall blade durability.
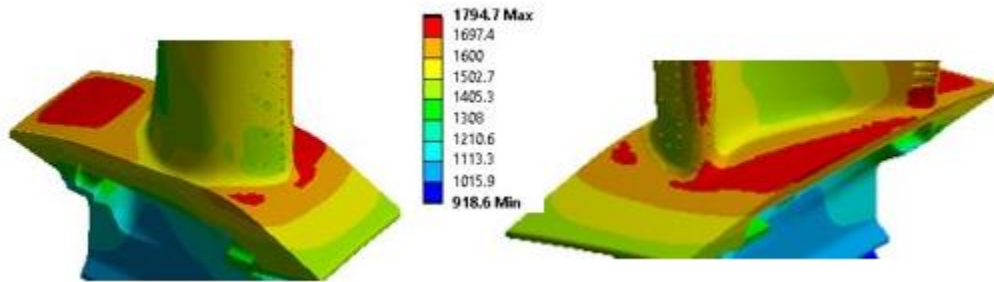
Figure 54 GP Stg1 Turbine Blade Metal Temperature
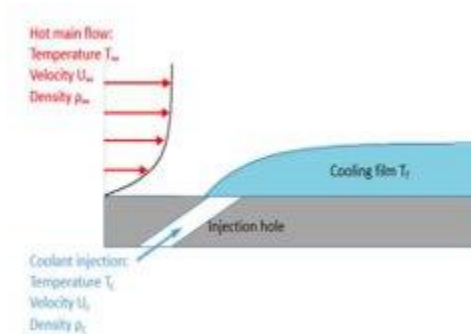
Figure 55 Platform Purge Flow Film Cooling [96]

4.2   Engine Operation Cycles and Blade Durability

Mechanical reliability is hugely impacted by the thermal distribution over the blade platform that need to be addressed during starts and shutdowns, which have impact on maximum temperature that is directly related to the creep hours capability that gets accelerated when coupled with higher platform surface temperature, also is has an impact on the fatigue capability which correlates to the high temp gradient over the platform surface.
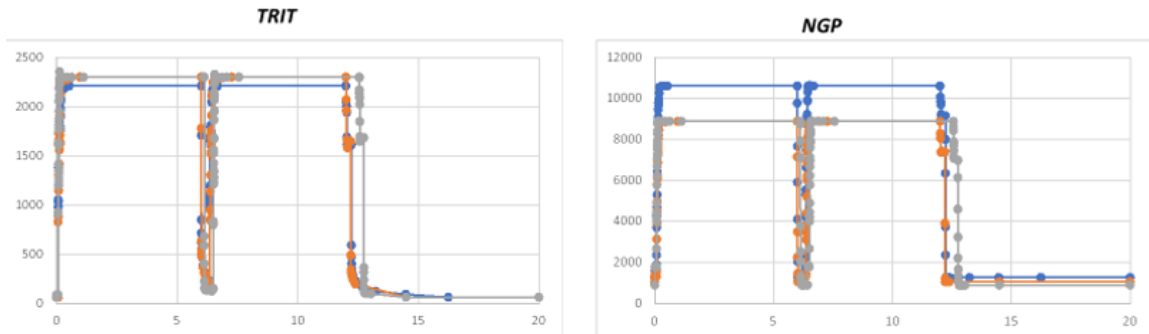
Figure 56 TRIT & Engine Speed Cycle

As we can notice in Fig 56, it is showing the change in the engine firing temperature during the engine operation, it can be noticed how critical it is and showing the severity of the operation conditions on GP blades temperature and engine speed during engine normal operation.

4.3   Future Work

4.3.1   Thermal Model Assessment (Case C 20% Delta Pressure Reduction)

Thermal model study is anticipated to follow this study in order to provide delta temperature data between baseline and contoured surface non-axisymmetric, platform contour will have an impact on the maximum temperature and creep hours life, in addition it will also cause changes in temperature gradient on the platform surface that is directly connected to the blade's fatigue life capability.

4.3.2   Experimental Test in 5 Blades Linear Cascade

This test will be presented in a future study to provide film cooling effectiveness distributions of blades platform passage to test effect of contoured platform on flow and platform film cooling effectiveness and validate it with CFD predictions.

The test will be performed using engine real conditions inlet and will match inlet upcoming Mach and Reynolds number that matches the geometry scale used for the test. Bleed

flow blowing ratio will be identified to determine the mass flow of the bleed as a percentage of mainstream flow, engine conditions purge flow will be set between 4-5 % of mainstream flow.

Taken PSP images will be the converted. For each test, 4 images will be required, (1) air injection; (2) N2 injection; (3) reference; (4) dark. Provided pictures will be postprocessed and film cooling effectiveness for different contoured platform configurations will be evaluated for blades platform optimization. Then postprocess results for each configuration and compare with CFD predictions outcome results from the current study.
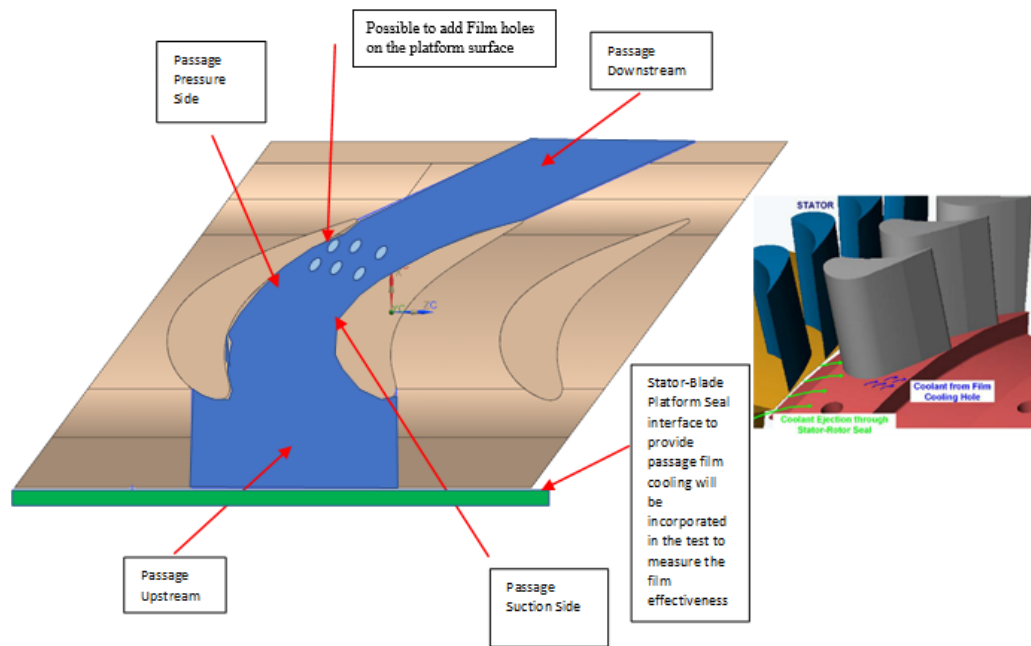
Figure 57 Platform Surface Axisymmetric Passage Between Blades and Bleed Injection Simulation

Stationary linear cascade can fit 5 blades, The scale used is 1:1. Main-stream flow is connected to a rectangular duct to supply air at a certain temperature, purge flow is supplied from the cavity between the platform specimen and bottom wall of the cascade as shown in the Figure 57 and Fig 58.
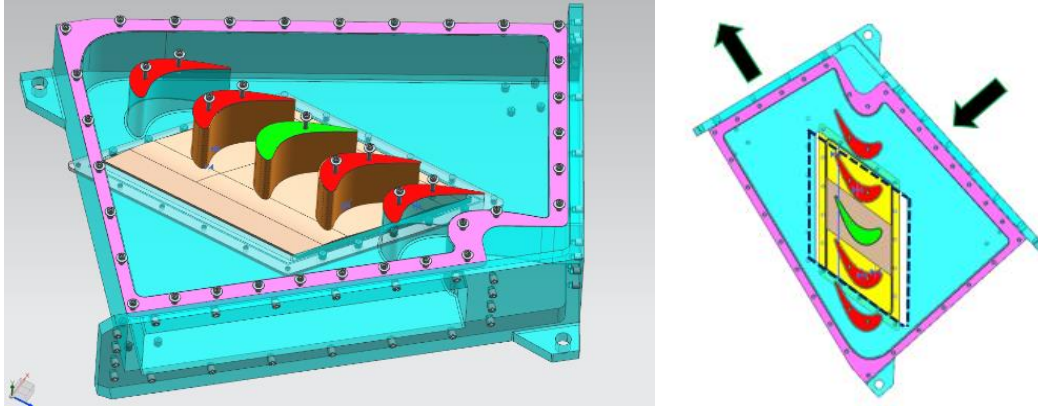
Figure 58 Linear Cascade Top and Isometric View

,

The second part of the future work study will be focusing on the mechanical and structural impact where structural & mechanical steady state structural ANSYS model will be created and study these geometric features combined with the new optimized cooling features applied to the platform surface to capture the change in overall blade durability and critical lifing against multiple failure variables such as stress concentrations (Kt), Low Cycle Fatigue (LCF) and Creep hours failure, The blade will be loaded with mechanical & thermal stresses.

Mechanical loads are primarily centrifugal force load, external & internal pressure distribution, static pressure distribution will be directly mapped to element faces using ANSYS commands that is extracted from a CFD analysis that has been, then perform a structural delta analysis for the baseline design and the new proposed blade design from durability and structural stand point (creep hours & fatigue cycles), the aim is to achieve an increase on hours of operation and increase cycles capability, there will be a concentration on the platform section using multiple design iterations between model changes, frequency analysis, thermal analysis and structural analysis in order to achieve the most optimized design.

The third part of the study will be High Cycle Fatigue (HCF) detailed study, Extensive

Modal Analysis will be built to extract blade natural frequencies and failure mode shapes,

assuring sufficient margins with the stimulus drivers with modified blade platform compared to

the baseline, this kind of analysis is requiring input from the structural model to get the non-

fluctuating mean stress (σ mean) and input from the blade MCS (Modal Cyclic Symmetry)

Analysis to capture the fluctuating alternative stress, alternative stresses (σ alternating) can be

then extracted from the Modal Cyclic Symmetry model for the blade in concern, this type of

analysis is more correlated to turbine blades because it works with objects that have a repetitive

pattern of parts.

REFERENCES

[1]   Mehdizadeh, M. (2014). A TOPSIS Method to Evaluate Different Types of Power Plants in IRAN with Overview of the Clean Development Mechanism (CDM). *New York Science Journal, 7*(10), 9-17.http://www.sciencepub.net/newyork/ny0710/003_27028ny071014_9_17.pdf

[2]   Boyce, M. P. (2012). Advanced industrial gas turbines for power generation. In *Combined Cycle Systems for Near-Zero Emission Power Generation* (pp. 44–102), Woodhead Publishing Limited. 10.1533/9780857096180.44

[3]   Langston, L. S., Nice, M. L., & Hooper, R. M. (1977). Three-Dimensional Flow Within a Turbine Cascade Passage. *Journal of Engineering for Power, 99*(1), 21-28. 10.1115/1.3446247

[4]   Martínez, A., Lara, G., Pascual, R., & López Droguett, E. (2014). Optimal Failure-Finding Intervals for Heat Shields in a Gas Turbine Combustion Chamber Using a Multicriteria Approach. *Journal of Engineering for Gas Turbines and Power, 137*(7), 072501. 10.1115/1.4029202

[5]   Flownex. (2020, July 21). *Aerospace*. https://www.flownex.com/legacy/industry-application/military-shipping-aerospace

[6]   Igoe, B., & Welch, M. (2014). Fuels, Combustion & Environmental Considerations in Industrial Gas Turbines. *Power Engineering, 118*(5), https://www.power-eng.com/coal/fuels-combustion-environmental-considerations-in-industrial-gas-turbines/#gref

[7]   Eduok, Y. (2013). *Chapter 20: F- Technology and Beyond*. In Y. Eduok (Ed.) Peaking Power (pp. 121-124). https://kupdf.net/download/ge-gas-turbines_59b2d9d4dc0d60ef64568edc_pdf

[8]   CCJ. (2014). CTOTF™: Addressing user concerns from the GT air inlet out to the transmission line. The Combined Cycle Journal. http://www.ccj-online.com/1q-2014/ctotf-addressing-user-concerns-from-the-gt-air-inlet-out-to-the-transmission-line/

[9]   Endeavor Precision. (2018). 7FA Stage one Nozzle. https://www.endeavorprecision.com/wp-content/uploads/2018/09/endeavor-PG-part-05-091318.jpg

[10]   Tristate Machinery Dismantlers. (n.d.). Ge frame 5 set 1ST stage turbine bucket *120 pristine*. http://www.tristatemachinerydismantlers.com/MICHIGAN/Motors-and-tools/Used/Ge-frame-5-set-1ST-stage-turbine-bucket-120-pristine.jsp

[11]   Kolagar, A. M., Tabrizi, N., Cheraghzadeh, M., & Shahriari, M. S. (2017). Failure analysis of gas turbine first stage blade made of nickel-based superalloy. *Case Studies in Engineering Failure Analysis, 8*, 61–68. 10.1016/j.csefa.2017.04.002

[12]   Rajabinezhad, M., Bahrami, A., Mousavinia, M., Seyedi, S. J., & Taheri, P. (2020). Corrosion-Fatigue Failure of Gas-Turbine Blades in an Oil and Gas Production Plant. *Materials, 13*(4), 900. 10.3390/ma13040900

[13]   Błachnio, J., & Pawlak, W. I. (2015). Non-Uniformity of the Combustor Exit Flow Temperature in Front of the Gas Turbine, 8(4), 209-213. https://doi.org/10.2478/ama-2014-0038

[14]   Narzary, D. P., Liu, K.-C., & Han, J.-C. (2012). Influence of Coolant Density on Turbine Blade Platform Film-Cooling. *Journal of Thermal Science and Engineering Applications, 4*(2), 021002. 10.1115/1.4005732.

[15]   Dickhoff, J., Kazari, M., & Tanaka, R. (2016). Improving cooling effectiveness of gas turbines through design exploration. Power Engineering International.

https://www.powerengineeringint.com/coal-fired/equipment-coal-fired/improving-cooling-effectiveness-of-gas-turbines-through-design-exploration/

[16]   Zhang, Z., Zhang, Y., Dong, X., Qu, X., Lu, X., & Zhang, Y. (2020). Flow mechanism between purge flow and mainstream in different turbine rim seal configurations. Chinese Journal of Aeronautics. 10.1016/j.cja.2020.02.016

[17]   Ligrani, P., Potts, G., & Fatemi, A. (2017). Endwall aerodynamic losses from turbine components within gas turbine engines. *Propulsion and Power Research, 6*(1), 1–14. 10.1016/j.jppr.2017.01.006

[18]   Bohn, D. E., Kusterer, K., Sürken, N., & Kreitmeier, F. (2000). Influence of Endwall Contouring in Axial Gaps on the Flow Field in a Four-Stage Turbine. *Volume 1: Aircraft Engine; Marine; Turbomachinery; Microturbines and Small Turbomachinery.* 10.1115/2000-gt-0472

[19]   Langston, L. S. (1980). Crossflows in a Turbine Cascade Passage. *Journal of Engineering for Power, 102*(4), 866–874. 10.1115/1.3230352

[20]   Langston, L. S. (2002). Secondary Flows in Axial Turbines-A Review. *Annals of the New York Academy of Sciences, 934*(1), 11–26. 10.1111/j.1749-6632.2001.tb05839.x

[21]   Chyu, M. K. (2001). Heat Transfer near Turbine Nozzle Endwall. *Annals of the New York Academy of Sciences, 934*(1), 27–36. 10.1111/j.1749-6632.2001.tb05840.x

[22]   Simon, T. W., & Piggush, J. D. (2006). Turbine Endwall Aerodynamics and Heat Transfer. *Journal of Propulsion and Power, 22*(2), 301–312. 10.2514/1.16344

[23]   Takeishi, K., Matsuura, M., Aoki, S., & Sato, T. (1990). An Experimental Study of Heat Transfer and Film Cooling on Low Aspect Ratio Turbine Nozzles. *Journal of Turbomachinery, 112*(3), 488–496. 10.1115/1.2927684

[24]   Harasgama, S. P., & Burton, C. D. (1992). Film Cooling Research on the Endwall of a Turbine Nozzle Guide Vane in a Short Duration Annular Cascade: Part 1—Experimental Technique and Results. *Journal of Turbomachinery, 114*(4), 734–740. 10.1115/1.2928026

[25]   Jabbari, M. Y., Marston, K. C., Eckert, E. R. G., & Goldstein, R. J. (1996). Film Cooling of the Gas Turbine Endwall by Discrete-Hole Injection. *Journal of Turbomachinery, 118*(2), 278–284. 10.1115/1.2836637

[26]   Friedrichs, S., Hodson, H. P., & Dawes, W. N. (1996). Heat Transfer Committee Best Paper of 1995 Award: Distribution of Film-Cooling Effectiveness on a Turbine Endwall Measured Using the Ammonia and Diazo Technique. *Journal of Turbomachinery, 118*(4), 613–621. 10.1115/1.2840916

[27]   Friedrichs, S., Hodson, H. P., & Dawes, W. N. (1997). Aerodynamic Aspects of Endwall Film-Cooling. *ASME Journal of Turbomachinery, 119*(4), 786–793. 10.1115/1.2841189

[28]   Friedrichs, S., Hodson, H. P., & Dawes, W. N. (1999). The Design of an Improved Endwall Film-Cooling Configuration. *Journal of Turbomachinery, 121*(4), 772–780. 10.1115/1.2836731

[29]   Blair, M. F. (1974). An Experimental Study of Heat Transfer and Film Cooling on Large-Scale Turbine Endwalls. *Journal of Heat Transfer, 96*(4), 524–529. 10.1115/1.3450239

[30]   Burd, S. W., Satterness, C. J., & Simon, T. W. (2000). Effects of Slot Bleed Injection Over a Contoured Endwall on Nozzle Guide Vane Cooling Performance: Part II — Thermal Measurements. *Volume 3: Heat Transfer; Electric Power; Industrial and Cogeneration.* 10.1115/2000-gt-0200

[31]   Granser, D., & Schulenberg, T. (1990). Prediction and Measurement of Film Cooling Effectiveness for a First-Stage Turbine Vane Shroud. *Volume 4: Heat Transfer; Electric Power; Industrial and Cogeneration.* 10.1115/90-gt-095

[32]   Oke, R., Simon, T., Shih, T., Zhu, B., Lin, Y. L., & Chyu, M. (2001). Measurements Over a Film-Cooled, Contoured Endwall with Various Coolant Injection Rates. *Volume 3: Heat Transfer; Electric Power; Industrial and Cogeneration.* 10.1115/2001-gt-0140

[33]   Oke, R. A., & Simon, T. W. (2002). Film Cooling Experiments with Flow Introduced Upstream of a First Stage Nozzle Guide Vane Through Slots of Various Geometries. *Volume 3: Turbo Expo 2002, Parts A and B.* 10.1115/gt2002-30169

[34]   Roy, R. P., Squires, K. D., Gerendas, M., Song, S., Howe, W. J., & Ansari, A. (2000). Flow and Heat Transfer at the Hub Endwall of Inlet Vane Passages — Experiments and Simulations. *Volume 3: Heat Transfer; Electric Power; Industrial and Cogeneration*. 10.1115/2000-gt-0198

[35]   Zhang, L. J., & Jaiswal, R. S. (2001). Turbine Nozzle Endwall Film Cooling Study Using Pressure-Sensitive Paint. *Journal of Turbomachinery, 123*(4), 730–735. 10.1115/1.1400113

[36]   Zhang, L., & Moon, H. K. (2004). Turbine Nozzle Endwall Inlet Film Cooling: The Effect of a Back-Facing Step and Velocity Ratio. *Heat Transfer, 1*, 1-10. 10.1115/imece2004-59117

[37]   Wright, L. M., Blake, S. A., Rhee, D.-H., & Han, J.-C. (2009). Effect of Upstream Wake with Vortex on Turbine Blade Platform Film Cooling with Simulated Stator-Rotor Purge Flow. *Journal of Turbomachinery, 131*(2), 021017. 10.1115/1.2952365

[38]   Gao, Z., Narzary, D. P., Mhetras, S., & Han, J. C. (2012). Upstream Vortex Effects on Turbine Blade Platform Film Cooling with Typical Purge Flow. *Journal of Thermophysics and Heat Transfer, 26*(1), 75–84. 10.2514/1.42411

[39]   Suryanarayanan, A., Ozturk, B., Schobeiri, M. T., & Han, J. C. (2010). Film-Cooling Effectiveness on a Rotating Turbine Platform Using Pressure Sensitive Paint Technique. *Journal of Turbomachinery, 132*(4), 041001-041013. 10.1115/1.3142860

[40]   Nicklas, M. (2001). Film-Cooled Turbine Endwall in a Transonic Flow Field: Part II—Heat Transfer and Film-Cooling Effectiveness. *Journal of Turbomachinery, 123*(4), 720–729. 10.1115/1.1397308

[41]   Wright, L. M., Gao, Z., Yang, H., & Han, J.-C. (2008). Film Cooling Effectiveness Distribution on a Gas Turbine Blade Platform with Inclined Slot Leakage and Discrete Film Hole Flows. *Journal of Heat Transfer, 130*(7), 071702, 1-11. 10.1115/1.2907440

[42]   Gao, Z., Narzary, D., & Han, J.-C. (2009). Turbine Blade Platform Film Cooling with Typical Stator-Rotor Purge Flow and Discrete-Hole Film Cooling. *Journal of Turbomachinery, 131*(4), 041004, 1-11. 10.1115/1.3068327

[43]   Suryanarayanan, A., Mhetras, S. P., Schobeiri, M. T., & Han, J. C. (2009). Film-Cooling Effectiveness on a Rotating Blade Platform. *Journal of Turbomachinery, 131*(1), 011014, 1-12. 10.1115/1.2752184

[44]   Wright, L. M., Blake, S., & Han, J.-C. (2007). Effectiveness Distributions on Turbine Blade Cascade Platforms Through Simulated Stator-Rotor Seals. *Journal of Thermophysics and Heat Transfer, 21*(4), 754–762. 10.2514/1.30382

[45]   Pedersen, D. R., Eckert, E. R. G., & Goldstein, R. J. (1977). Film Cooling with Large Density Differences Between the Mainstream and the Secondary Fluid Measured by the Heat-Mass Transfer Analogy. *Journal of Heat Transfer, 99*(4), 620–627. 10.1115/1.3450752

[46]   Sinha, A. K., Bogard, D. G., & Crawford, M. E. (1991). Film-Cooling Effectiveness Downstream of a Single Row of Holes with Variable Density Ratio. *Journal of Turbomachinery, 113*(3), 442–449. 10.1115/1.2927894

[47]   Ethridge, M. I., Cutbirth, J. M., & Bogard, D. G. (2001). Scaling of Performance for Varying Density Ratio Coolants on an Airfoil with Strong Curvature and Pressure Gradient Effects. *Journal of Turbomachinery, 123*(2), 231–237. 10.1115/1.1343457

[48]   Ekkad, S. V., Mehendale, A. B., Han, J. C., & Lee, C. P. (1997). Combined Effect of Grid Turbulence and Unsteady Wake on Film Effectiveness and Heat Transfer Coefficient of a Gas Turbine Blade with Air and CO2 Film Injection. *Journal of Turbomachinery, 119*(3), 594–600. 10.1115/1.2841163

[49]   Kadotani, K., & Goldstein, R. J. (1979). On The Nature of Jets Entering a Turbulent Flow: Part A—Jet–Mainstream Interaction. *Journal of Engineering for Power, 101*(3), 459–465. 10.1115/1.3446601

[50]   Jumper, G. W., Elrod, W. C., & Rivir, R. B. (1991). Film Cooling Effectiveness in High-Turbulence Flow. *Journal of Turbomachinery, 113*(3), 479–483. 10.1115/1.2927899

[51]   Bons, J. P., MacArthur, C. D., & Rivir, R. B. (1996). The Effect of High Free-Stream Turbulence on Film Cooling Effectiveness. *Journal of Turbomachinery, 118*(4), 814–825. 10.1115/1.2840939

[52]   Schmidt, D. L., & Bogard, D. G. (1996). Effects of Free-Stream Turbulence and Surface Roughness on Film Cooling. *Volume 4: Heat Transfer; Electric Power; Industrial and Cogeneration.* 10.1115/96-gt-462

[53]   Burd, S. W., Kaszeta, R. W., & Simon, T. W. (1998). Measurements in Film Cooling Flows: Hole L/D and Turbulence Intensity Effects. *Journal of Turbomachinery, 120*(4), 791–798. 10.1115/1.2841791

[54]   Praisner, T. J., & Smith, C. R. (2006). The Dynamics of the Horseshoe Vortex and Associated Endwall Heat Transfer—Part I: Temporal Behavior. *Journal of Turbomachinery, 128*(4), 747-754. 10.1115/1.2185676

[55]   Zhang, Y., & Yuan, X. (2011). Film Cooling Effectiveness Distribution on First-Stage Vane Endwall with and Without Leading-Edge Fillets: Part I—Effect of Leading Edge Geometry. *Volume 5: Heat Transfer, Parts A and B.* 10.1115/gt2011-45427

[56]   Zhang, Y., Yuan, X., & Ligrani, P. (2013). Film cooling effectiveness distribution on first-stage vane endwall with and without leading-edge fillets. *International Journal of Heat and Mass Transfer, 66*, 642–654. 10.1016/j.ijheatmasstransfer.2013.06.065

[57]   Mahmood, G. I., Gustafson, R., & Acharya, S. (2005). Experimental Investigation of Flow Structure and Nusselt Number in a Low-Speed Linear Blade Passage with and Without Leading-Edge Fillets. *Journal of Heat Transfer, 127*(5), 499-512. 10.1115/1.1865218

[58]   Han, S., & Goldstein, R. J. (2006). Influence of Blade Leading Edge Geometry on Turbine Endwall Heat (Mass) Transfer. *Journal of Turbomachinery, 128*(4), 798-813. 10.1115/1.2221326

[59]   Burd, S. W., & Simon, T. W. (2000). Effects of Slot Bleed Injection over a

Contoured Endwall on Nozzle Guide Vane Cooling Performance: Part I – Flow Field

Measurements. *ASME, 2000-GT-199*.

[60]   Oke, R. A., Simon, T. W., Burd, S. W., & Vahlberg, R. (2000). Measurements in

a Turbine Cascade Over a Contoured Endwall: Discrete Hole Injection of Bleed Flow. *Volume 3:*

Heat Transfer; Electric Power; Industrial and Cogeneration. 10.1115/2000-gt-0214

[61]   Zhang, L., & Moon, H. K. (2003). Turbine Nozzle Endwall Inlet Film Cooling:

The Effect of a Back-Facing Step. *Volume 5: Turbo Expo 2003, Parts A and B.* 10.1115/gt2003-

38319

[62]   Kopper, F. C., Milanot, R., & Vancot, M. (1981). Experimental Investigation of

Endwall Profiling in a Turbine Vane Cascade. *AIAA Journal, 19*(8), 1033–

1040. 10.2514/3.51032

[63]   Boyle, R. J., & Haas, J. E. (1982). Comparison of Experimental and Analytical

Performance for Contoured Endwall Stators. *Paper, AIAA-82-1286*.

[64]   Moustapha, S. H., & Williamson, R. G. (1986). Effect of two endwall contours on

the performance of an annular nozzle cascade. *AIAA Journal, 24*(9), 1524–1530. 10.2514/3.9475

[65]   Becz, S., Majewski, M. S., & Langston, L. S. (2003). Leading Edge Modification

Effects on Turbine Cascade Endwall Loss. *Volume 6: Turbo Expo 2003, Parts A and*

B. 10.1115/gt2003-38898

[66]   Saha, A. K., Mahmood, G. I., & Acharya, S. (2006). The Role of Leading-Edge

Contouring on End-Wall Flow and Heat Transfer: Computations and Experiments. *Volume 3:*

Heat Transfer, Parts A and B. 10.1115/gt2006-91318

[67]   Shih, T. I.-P., & Lin, Y.-L. (2003). Controlling Secondary-Flow Structure by Leading-Edge Airfoil Fillet and Inlet Swirl to Reduce Aerodynamic Loss and Surface Heat Transfer. *Journal of Turbomachinery, 125*(1), 48-56. 10.1115/1.1518503

[68]   Zess, G. A., & Thole, K. A. (2002). Computational Design and Experimental Evaluation of Using a Leading Edge Fillet on a Gas Turbine Vane. *Journal of Turbomachinery, 124*(2), 167-175. 10.1115/1.1460914

[69]   Knezevici, D. C., Sjolander, S. A., Praisner, T. J., Allen-Bradley, E., & Grover, E. A. (2009). Measurements of Secondary Losses in a High-Lift Front-Loaded Turbine Cascade with the Implementation of Non-Axisymmetric Endwall Contouring. *Volume 7: Turbomachinery, Parts A and B.* 10.1115/gt2009-59677

[70]   Lynch, S. P., Sundaram, N., Thole, K. A., Kohli, A., & Lehane, C. (2009). Heat Transfer for a Turbine Blade with Non-Axisymmetric Endwall Contouring. *Volume 3: Heat Transfer, Parts A and B,* 887-898. doi:10.1115/gt2009-60185

[71]   Snedden, G., Dunn, D., Ingram, G., & Gregory-Smith, D. (2009). The Application of Non-Axisymmetric Endwall Contouring in a Single Stage, Rotating Turbine. *Volume 7: Turbomachinery, Parts A and B.* 10.1115/gt2009-59169

[72]   Zhang, L., & Moon, H. K. (2011). Comparison of Two Axisymmetric Profiles on Blade Platform Film Cooling. *Volume 5: Heat Transfer, Parts A and B,* 11-20.10.1115/gt2011-45102.

[73]   Erickson, R. D., Simon, T. W, Zhang, L. J., & Moon, H. K. (2011). Experimental Investigation of Disk Cavity Leakage Flow and Hub Endwall Contouring in a Linear Rotor Cascade. *ASME,* GT2011-45102.

[74]   Zhang, L., Lee, D. H., Yin, J., & Moon, H. K. (2013). The Effect of Axisymmetric Profile on Turbine Blade Platform Heat Transfer Distribution. *Volume 3C: Heat Transfer*. 10.1115/gt2013-94335.

[75]   Sangston, K., Little, J., Eric Lyall, M., & Sondergaard, R. (2016). Effect of Blade Profile Contouring on Endwall Flow Structure in a High-Lift Low-Pressure Turbine Cascade. *Journal of Turbomachinery, 139*(2), 021006. 10.1115/1.403448.

[76]   Li, S.-J., Lee, J., Han, J.-C., Zhang, L., & Moon, H.-K. (2016). Influence of mainstream turbulence on turbine blade platform cooling from simulated swirl purge flow. *Applied Thermal Engineering, 101,* 678–685. 10.1016/j.applthermaleng.2016

[77]   Rouina, S., Abdeh, H., Barigozzi, G., Odemondo, V., Abba, L., & Iannone, M. (2021). Film Cooling Effectiveness Measurement of Fan-Shaped Holes Manufactured Using EDM Technique. *Journal of Turbomachinery, 144*(7). 10.1115/1.4053236

[78]   Chen, A. F., Shiau, C.-C., & Han, J.-C. (2017). Turbine Blade Platform Film Cooling with Fan-Shaped Holes Under Simulated Swirl Purge Flow and Slashface Leakage Conditions. *Volume 5C: Heat Transfer.* 10.1115/gt2017-63119

[79]   Ahn, J., Schobeiri, M. T., Han, J.-C., & Moon, H.-K. (2004). Film Cooling Effectiveness on the Leading Edge of a Rotating Turbine Blade. *Heat Transfer, 1*. 10.1115/imece2004-59852

[80]   Ahn, J. Y., Schobeiri, M. T., Han, J. C., & Moon, H. K. (2006). Film Cooling Effectiveness on the Leading Edge of a Rotating Film-Cooled Blade Using Pressure Sensitive Paint. *ASME J. Heat Transfer, 128*(9), 879–888.

[81]   Ahn, J., Schobeiri, M. T., Han, J.-C., & Moon, H.-K. (2007). Effect of rotation on leading edge region film cooling of a gas turbine blade with three rows of film cooling holes.

International Journal of Heat and Mass Transfer, 50(1-2), 15–

25. 10.1016/j.ijheatmasstransfer.2006.06.028

[82]   Schuepbach, P., Abhari, R. S., Rose, M. G., & Gier, J. (2009). Influence of Rim

Seal Purge Flow on Performance of an Endwall-Profiled Axial Turbine. *Volume 7:*

Turbomachinery, Parts A and B, 943-956. 10.1115/gt2009-59653

[83]   Jenny, P., Abhari, R. S., Rose, M. G., Brettschneider, M., & Gier, J. (2012). A

Low Pressure Turbine With Profiled Endwalls and Purge Flow Operating With a Pressure Side

Bubble. *Journal of Turbomachinery, 134*(6), 061038. 10.1115/1.4006303

[84]   Schobeiri, M. T., & Lu, K. (2011). Endwall Contouring Using Continuous

Diffusion: A Breakthrough Method and its Application to a Three-Stage High Pressure Turbine.

Volume 7: Turbomachinery, Parts A, B, and C, 787-797. 10.1115/gt2011-45931

[85]   Eymann, S., Reinmöller, U., Niehuis, R., Förster, W., Beversdorff, M., & Gier, J.

(2002). Improving 3D Flow Characteristics in a Multistage LP Turbine by Means of Endwall

Contouring and Airfoil Design Modification: Part 1 — Design and Experimental Investigation.

Volume 5: Turbo Expo 2002, Parts A and B, 249-260. 10.1115/gt2002-30352

[86]   Hartland, J., & Gregory-Smith, D. (2002). A Design Method for the Profiling of

Endwalls in Turbines. *Volume 5: Turbo Expo 2002, Parts A and B*, 697-704. 10.1115/gt2002-

30433

[87]   Ingram, G., Gregory-Smith, D., Rose, M., Harvey, N., & Brennan, G. (2002). The

Effect of End-Wall Profiling on Secondary Flow and Loss Development in a Turbine Cascade.

Volume 5: Turbo Expo 2002, Parts A and B, 135-145. 10.1115/gt2002-30339

[88]   Sauer, H., Müller, R., & Vogeler, K. (2001). Reduction of Secondary Flow Losses in Turbine Cascades by Leading Edge Modifications at the Endwall. *Journal of Turbomachinery, 123*(2), 207-213. 10.1115/1.1354142

[89]   Brennan, G., Harvey, N. W., Rose, M. G., Fomison, N., & Taylor, M. D. (2001). Improving the Efficiency of the Trent 500 HP Turbine Using Non-Axisymmetric Endwalls: Part 1 — Turbine Design. *Volume 1: Aircraft Engine; Marine; Turbomachinery; Microturbines and Small Turbomachinery*. doi:10.1115/2001-gt-0444

[90]   Harvey, N. W., Brennan, G., Newman, D. A., & Rose, M. G. (2002). Improving Turbine Efficiency Using Non-Axisymmetric Endwalls: Validation in the Multi-Row Environment and With Low Aspect Ratio Blading. *Volume 5: Turbo Expo 2002, Parts A and B,* 119-126. 10.1115/gt2002-30337

[91]   Germain, T., Nagel, M., Raab, I., Schuepbach, P., Abhari, R. S., & Rose, M. (2008). Improving Efficiency of a High Work Turbine Using Non-Axisymmetric Endwalls: Part I—Endwall Design and Performance. *Volume 6: Turbomachinery, Parts A, B, and C, 1109-1119.* 10.1115/gt2008-50469

[92]   Snedden, G., Dunn, D., Ingram, G., & Gregory-Smith, D. (2010). The Performance of a Generic Non-Axisymmetric Endwall in a Single Stage, Rotating Turbine at On and Off-Design Conditions. *Volume 7: Turbomachinery, Parts A, B, and C,* 1069-1080. 10.1115/gt2010-22006

[93]   Schobeiri, M. T. (2012). *Aerodynamics and Heat Transfer Studies of Parameters Specific to the IGCC-Requirements: Endwall Contouring, Leading Edge Filleting and Blade Tip Ejection Under Rotating Turbine Conditions Advanced Turbine Program.* U.S. Department of Energy Quarterly Report 2012, Period of Performance: May 01/2012 to July 31/2012

[94] Schobeiri, M. T., Lu, K., & Han, J. C. (2012). Numerical Investigation of the Effect of Purge Flow on Aerodynamic Performance and Film Cooling Effectiveness on a Rotating Turbine with Non-Axisymmetric Endwall Contouring. *Volume 4: Heat Transfer, Parts A and B,* 413-423. 10.1115/gt2012-69069

[95] Han, J.-C. (2013). Fundamental Gas Turbine Heat Transfer. *Journal of Thermal Science and Engineering Applications, 5*(2), 021007. 10.1115/1.4023826

[96] Xue, S., & Ng, W. (2018). Turbine Blade Tip External Cooling Technologies. *Aerospace, 5*(3), 90. 10.3390/aerospace5030090